Journal of Molecular Catalysis A: Chemical 355 (2012) 44–60

Contents lists available at SciVerse ScienceDirect

Journal of Molecular Catalysis A: Chemical

journal homepage: www.elsevier.com/locate/molcata

Editor's choice paper

Experimental design and MM2–PM6 molecular modelling of hematin as a peroxidase-like catalyst in Alizarin Red S degradation

Agostina Córdoba[a,*], Ivana Magario[a,1], María Luján Ferreira[b,2]

[a] Investigación y Desarrollo en Tecnología Química (IDTQ), Grupo Vinculado PLAPIQUI – CONICET, Facultad de Ciencias Exactas, Físicas y Naturales, Universidad Nacional de Córdoba, Av. Vélez Sarsfield 1611, X5016GCA, Ciudad Universitaria, Córdoba, Argentina

[b] Planta Piloto de Ingeniería Química (PLAPIQUI), PLAPIQUI-UNS-CONICET, Universidad Nacional del Sur, Camino La Carrindanga Km 7, CC 717, 8000 Bahía Blanca, Provincia de Buenos Aires, Argentina

ARTICLE INFO

Article history:
Received 21 October 2011
Received in revised form
30 November 2011
Accepted 7 December 2011
Available online 16 December 2011

Keywords:
Alizarin Red S
Hematin
Horseradish peroxidase
Molecular modelling
Doehlert

ABSTRACT

A combined experimental design and molecular modelling study of the efficiency of hematin/HRP–H_2O_2 in Alizarin Red S (ARS) removal from aqueous solutions is reported. A Doehlert experimental design using 21 experiments, with temperature range fixed to 30–50 °C, pH range 7–11, hydrogen peroxide concentration from 0.05 to 5 mM and catalyst concentration from 0.05 to 4.95 mg/l is used. The factor levels are 7 for H_2O_2 concentration and pH, 5 for temperature and 3 for catalyst concentration. At optimal conditions, 75 mg/l ARS solutions are totally decolorized by hematin whereas HRP only achieves 57% conversion.

UV/visible spectra analysis of reaction medium, species profiles during reaction using HRP/hematin at selected conditions and molecular modelling using molecular mechanics (MM2) and semiempirical studies (PM6-MOPAC 2009) are presented and discussed to explain the experimental findings. Cpd-I of HRP coordinates selectively ARS vs. hydrogen peroxide. Dimers of ARS may inhibit HRP. ARS may be coordinated by different hydroxyls to hematin depending on the availability of them, considering the pH. Catalatic reaction is important in the case of hematin but it is not in the case of HRP in our range of experimental conditions.

1. Introduction

Horseradish peroxidase (HRP) catalyzes oxidative polymerization of phenol and aniline [1,2]. Many dyes may be seen as phenol derivatives, because they have anthraquinonic structures. One of them is Alizarin Red S (ARS) (Fig. 1, see the hydroxyls groups called 1 and 2). ARS is used by textile industry and for histochemical staining [3]. Anthraquinone dyes like ARS are recalcitrant and durable pollutants in the aquatic ecosystems, where they are disposed in wastewaters. The classical dye degradation processes based on chemical, physical and biological oxidation are not always efficient enough. New approaches using photocatalytic [4] and electrochemical [5] processes are often expensive. Enzymatic treatment of aqueous solutions of phenols and dyes using systems based on peroxidases has been reported, soluble [6–9] and immobilized [10–14]. These enzymatic methods are also expensive and affected by the sensitivity of the enzymes to the environment – pH and other pollutants – [15]. Due to the enzymes high cost and sensitivity to inhibition or degradation, the idea of a cheaper although effective catalyst that may function similarly or even more efficiently than enzymes is very attractive.

One group of these cheaper alternatives to HRP are metalloporphyrins and particularly iron porphyrins [16,17]. Hematin, a hydroxyferriprotoporphyrin, is the more stable oxidized form of the free heme. The use of hematin as a catalyst for oxidative polymerization reactions is not widespread due to the low solubility at acidic conditions [18]. Strategies such as chemical modification or immobilization of hematin have been proposed to overcome these problems [19,20].

Combined experimental–theoretical studies in the field of enzymatic–biomimetic oxidative degradation of phenol derivatives are really scarce [21] even when the molecular mechanics version 2 (MM2) and semiempirical methods (parameterized method 6 or PM6 from MOPAC 2009) have been applied from long time ago to study metalloporphyrins [22,23] and HRP. In the case of HRP, electronic and steric characteristics of Cpd-I, Cpd-II and

* Corresponding author. Tel.: +54 0 351 4334141x220.
E-mail addresses: agostinacordoba@gmail.com (A. Córdoba), imagario@efn.uncor.edu (I. Magario), mlferreira@plapiqui.edu.ar (M.L. Ferreira).
[1] Tel.: +54 0 351 4334141x191.
[2] Tel.: +54 0 291 4861700x261.

1381-1169/$ – see front matter © 2011 Elsevier B.V. All rights reserved.
doi:10.1016/j.molcata.2011.12.011

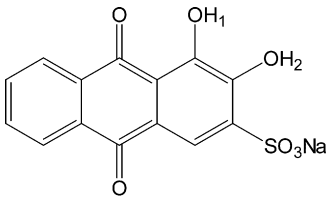

Fig. 1. Alizarin Red S chemical structure (C.I.:58005).

Cpd-III have been reported using ab-initio methods and also docking studies with selected substrates [24–27].

Sophisticated approaches have been applied to study different substrates and their interaction with peroxidases [28]. Structural studies with theoretical molecular modelling have been combined to study the interaction of certain molecules as substrates of HRP [29]. Studies of the interaction of hematin with phenolic substrates for oxidative reactions are not common.

The first step for a complete study of ARS degradation using HRP–hematin is to analyze differences and similarities in the activity in ARS conversion in a comparative way. Some of our group have studied at selected conditions the degradation of Alizarin with soluble HRP and hematin using the one-factor-at-a-time (OFAT) approach [7] and this work is the continuation of that former work. Taking into account the previous experimental work, we present results obtained for ARS using Doehlert optimization in buffered aqueous solutions to explore the impact of pH, temperature, hydrogen peroxide and hematin/HRP concentration in two responses: ARS conversion and catalytic yield. UV/vis spectra changes of reaction systems with time as well as oxygen and peroxide time profiles during reaction are also analyzed to give insights into the reaction mechanisms of both catalysts.

Besides, using simple MM2 plus PM6 molecular modelling of hematin and HRP and their interaction with substrates, some key aspects on the mechanism of interaction of both catalysts with hydrogen peroxide and ARS are explored. The goal is to give support to the explanations of our experimental findings.

2. Experimental

2.1. Materials

Horseradish peroxidase (HRP) was kindly provided by Amano Inc. (Elgin, USA) and was used without further purification. The enzyme has a molecular weight of 41,000 Da, a stable pH range from pH 6 to 10 and a catalytic activity higher than 180 U/mg for the 4-aminoantipyrine/phenol reaction (Amano Inc., datasheet). Hematin (633.49 molecular mass) from Sigma Co. (San Luis, USA) was employed as provided. ARS (C.I.:58005) with a λ_{max} = 511 nm, was supplied by Farmitalia Carlo Erba, Montedison Group (Milano, Italia) and used without purification. Buffer solutions were prepared with distilled water and salts of analytical grade. Hydrogen peroxide 30 vol.% (2.68 mM) was provided by Apotarg S.R.L. Laboratories (Córdoba, Argentina).

2.2. Decolorization reaction

Reactions were carried out using 10 ml glass vials inside a thermal bath and under magnetic stirring. The initial dye concentration was kept constant at 75 mg/l (0.22 mM) in all experiments. The dye solution was prepared in 0.1 M phosphate buffer for the 7.4–7.8 pH-range; using 0.1 M Tris for 8.6–9.4 pH-range and 0.1 M carbonate/bicarbonate solutions for pH values higher than 10. In all cases the counter-ion was sodium. An HRP solution was prepared by dissolving 4.62 mg in 9240 μl of 0.1 M sodium phosphate buffer pH 7.0 (500 mg/l). The hematin solution contained 8.1 mg of hematin in 25 ml of 0.01 M NaOH solution (324 mg/l). The reaction mixture consisted of 5150 μl of 150 mg/l ARS solution, a corresponding volume of HRP or hematin solution (11.5–141 μl) and the required amount of buffer to reach a final volume of 10.3 ml. Commercial hydrogen peroxide 30 vol.% (1.4–5 μl) was added stepwise at 0, 10 and 20 min of reaction time to minimize inactivation effects. Two 300 μl samples were withdrawn; one before first hydrogen peroxide addition and the other after 60 min of reaction. The samples were immediately diluted in 2.7 ml buffer solution and analyzed by UV–visible spectroscopy. The evaluation of the treatment efficiency was carried out through absorbance readings at 511 nm; however, spectra were recorded in a 200–800 nm range. A Perkin-Elmer Lambda 35 spectrophotometer (Massachusetts, USA) was used for all measurements.

2.3. Experimental design

In order to evaluate performances of both catalysts within a specific region of reaction conditions (i.e. setting ranges of the independent variables) an experimental design was selected based on response surface methodology (RSM) [30,31]. Thus, multivariate polynomial models were obtained from experimental data (measured responses) by least-square estimates. Experimental responses were fitted to the following quadratic model:

$$Y = b_0 + \sum b_i \cdot X_i + \sum b_{ii} \cdot X_i^2 + \sum \sum b_{ij} \cdot X_i \cdot X_j \quad (1)$$

where Y is the predicted response, b_0 is the average of all experimental responses, b_i the main effect coefficient of the variable X_i, b_{ii} the second-order coefficient of the variable X_i, and b_{ij} the interaction effect coefficient between variables X_i and X_j ($i \neq j$). Variables and their interactions effects as well as curvature effects on the response were thereby statistically evaluated. A Doehlert design [32] with four factors was applied in order to estimate the parameters of Eq. (1). Doehlert arrays are shell designs based on regular simplex and have the particularity of having an equally spaced points distribution [32]. In contrast to familiar designs, Doehlert arrays are more uniform (number of experiments equal to $k^2 + k + 1$, being k the number of factors). This set allows a stepwise approach. In a first step the effects of a group of factors are evaluated extending then the analysis to more variables in a second step, through the expansion of the experimental matrix [33,34]. Thus, the effects of the pH of reaction medium, temperature, and H_2O_2 concentration were first analyzed. To this goal, the experimental matrix had thirteen experiments uniformly distributed that may be represented in normalized variables (X_i) by the apexes and center of a cube-octahedron (Table 1, experiments 1–13) [32]. In a second step, the catalyst concentration was varied as an additional independent variable. Thus, eight experiments were added to the Doehlert array (Table 1, experiments 14–21). The central point was carried out four times to evaluate the reproducibility of the responses. The experimental order in each step was done randomly; however, the experiments with the same temperature were joined together. Experimental region was defined considering preliminary results as well as pH and temperature conditions of effluents of the textile industry [35–37]. Thus, temperature range was fixed to 30–50 °C and pH range was 7–11. The hydrogen peroxide concentration ranged from 0.05 to 5 mM, so the molar ratio H_2O_2/ARS varied from 0.23 to 23. The catalyst concentration was modified between 0.05 to 4.95 mg/l, which means a variation of mass ratio catalyst/ARS from 6×10^{-4} to 6×10^{-2}. The factor levels were as follows: 7 for H_2O_2 concentration and pH, 5 for temperature and 3 for catalyst concentration.

The values of the variables are coded or normalized as $X_i = (U_i - U_M)/\Delta U$; where X_i is the normalized variable with range

Table 1
Doehlert array of experiments for four variables.

Exp.	Temperature		H_2O_2 concentration		pH value		Catalyst concentration	
	Effective (°C)	Coded	Effective (mM)	Coded	Effective (−)	Coded	Effective (mg/l)	Coded
1	40	0	2.5	0	9.0	0	2.5	0
2	50	+1.0000	2.5	0	9.0	0	2.5	0
3	45	+0.5000	4.7	+0.8660	9.0	0	2.5	0
4	35	−0.5000	4.7	+0.8660	9.0	0	2.5	0
5	45	+0.5000	3.2	+0.2887	10.6	+0.8165	2.5	0
6	35	−0.5000	3.2	+0.2887	10.6	+0.8165	2.5	0
7	40	0	1.1	−0.5774	10.6	+0.8165	2.5	0
8	30	−1.0000	2.5	0	9.0	0	2.5	0
9	35	−0.5000	0.4	−0.8660	9.0	0	2.5	0
10	45	+0.5000	0.4	−0.8660	9.0	0	2.5	0
11	35	−0.5000	1.8	−0.2887	7.4	−0.8165	2.5	0
12	45	+0.5000	1.8	−0.2887	7.4	−0.8165	2.5	0
13	40	0	4.0	+05774	7.4	−0.8165	2.5	0
Extended matrix for coupling catalyst concentration								
14	45	+0.5000	3.2	+0.2887	9.4	+0.2041	4.44	+0.7906
15	35	−0.5000	3.2	+0.2887	9.4	+0.2041	4.44	+0.7906
16	40	0	1.1	−0.5774	9.4	+0.2041	4.44	+0.7906
17	40	0	2.5	0	10.2	+0.6124	4.44	+0.7906
18	35	−0.5000	1.8	−0.2887	8.6	−0.2041	0.56	−0.7906
19	45	+0.5000	1.8	−0.2887	8.6	−0.2041	0.56	−0.7906
20	40	0	4.0	+0.5774	8.6	−0.2041	0.56	−0.7906
21	40	0	2.5	0	7.8	−0.6124	0.56	−0.7906
Repetitions at the center of the experimental region								
22–24	40	0	2.5	0	9.0	0	2.5	0

from −1 to +1, U_i the value of the effective variable, U_M the value at the center of the variable range and ΔU the step (=$(U_{i,Max} - U_{i,Min})/2$).

The selected responses were the percentage conversion (Y) and the catalytic yield (Z) defined as:

$$Y = \left(\frac{A_0 - A_{60}}{A_0}\right) \times 100 \quad (2)$$

$$Z = \frac{Y \cdot [\text{ARS}]}{100 \cdot [\text{Catalyst}] \cdot [H_2O_2] \cdot V_t} \quad (3)$$

where A_0 is the absorbance at cero time and A_{60} is the absorbance at 60 min of reaction. [ARS] and [H_2O_2] are in mM, V_t in liters and [catalyst] in g/l. The catalytic yield Z represents the milimols of converted ARS per gram of catalyst, per milimol of oxidant.

2.4. Statistical analysis

Statgraphics Centurion, version XV.2 (Virginia, USA) was employed to perform the statistical analysis of experimental data. Quadratic models which fit the studied responses have been obtained by multiple regressions. By developing Eq. (1) to the studied case, the complete set of factors and their interactions was first subjected to significance evaluation by the ANOVA test. The resulting non-statistical factors were suppressed and the fitting procedure was repeated until significance and goodness of fit (good R^2 values) were accomplished.

2.5. UV–visible analysis of hematin and HRP with H_2O_2

For the evaluation of the coordination of H_2O_2 with the Fe^{3+} in HRP and hematin the reaction with hydrogen peroxide without ARS was studied. The reaction was carried out in a quartz cuvette. The hematin/HRP concentration in cuvette was 5 mg/l. A single addition of 0.62 μl or 5.26 μl of H_2O_2 30 vol.% solution was employed to evaluate hydrogen peroxide effect at 0.56 and 4.7 mM respectively. The pH was set at 10, and the buffer concentration was 0.1 M when the catalyst is hematin and 0.01 M when the catalyst is HRP. The UV–vis spectra were measured before H_2O_2 addition, immediately after the peroxide addition and during the reaction up to 60 min of reaction with intervals of few minutes. A Perkin-Elmer Lambda 35 spectrophotometer (Massachusetts, USA) was used for all measurements.

2.6. Dissolved oxygen, H_2O_2 and ARS concentration profiles

Dissolved oxygen profiles were measured with a Pasco Pasport Dissolved Oxygen Sensor model PS-2108 (California, USA). Reactions were carried out with magnetic stirring at 30 °C. Selected experimental conditions were: catalyst concentration: 4 mg/l; hydrogen peroxide concentration: 2.5 mM, ARS concentration: 75 mg/l and medium pH: 9. 46.6 μl of 30 vol.% hydrogen peroxide was added in one step to 49.55 ml of ARS 75 mg/l in pH 9 buffer (Tris) solution. 400 μl of 500 mg/l HRP row solution was added to HRP/ARS system and 361.5 μl of 553.2 mg/l hematin row solution was added to hematin/ARS system. The oxygen measurement was continuous during near 60 min of reaction.

To obtain the hydrogen peroxide concentration versus time profiles, samples have been taken at different times of reaction. 1 ml sample was added to 8 ml of distilled water and 1 ml of H_2SO_4 1 M solution to stop the reaction. The H_2O_2 concentration in each sample was measured through iodometric titration [38].

For ARS oxidation reaction profiles, the reaction medium contained 9.33 μl of 30 vol.% hydrogen peroxide, 9.91 ml of ARS 75 mg/l in pH 9 buffer (Tris) solution and 80 μl of 500 mg/l HRP row solution for HRP/ARS system and 72.3 μl of 553.2 mg/l hematin row solution for hematin/ARS systems. Samples were withdrawn at different times after peroxide addition and treated as specified above (see Section 2.2). Conversions were calculated with Eq. (2) and multiplied by the ARS initial concentration to accomplish concentrations values.

2.7. HRP and hematin molecular modelling using MM2 and PM6

The model for HRP is based on the PDB 1H5A structure, from PDB [39]. It includes all the main residues that are thought to be involved in the catalytic mechanism plus the aromatic binding site [40]. The following residues are included in the molecular mechanics version 2 (MM2) plus the parameterized model 6 (PM6-MOPAC

2009) semiempirical calculation using hematin and a model of HRP, based on the most recent literature on the topic [41].

- Bonded to Fe from the protein: His170, Asp247.
- Two Ca^{2+} atoms, one distal and the other proximal, modelled as dummy atoms.
- Distal O donors: Asp43, Asp50, Ser52, Asp43, Val46, Gly48.
- Proximal O donor: Th171, Asp222, Thr225, Asp230, Ile228.
- Key residues for catalytic function: His42, Arg38, Phe41, Asn70, Pro139.
- Aromatic substrate binding: Phe68, Gly69, Pro139, Ala140, Phe142, Phe179.

The research on the mechanistic pathway of HRP has been very active last 30 years, from the experimental and also the theoretical point of view. The general mechanism of interaction with H_2O_2 – phenolic substrate, simplified, is presented generally in three steps. A first one with the generation of a water molecule and Cpd-I by reaction of HRP with H_2O_2, a second one with the interaction of Cpd-I with an aromatic substrate (AH) with the generation of Cpd-II and a radical $A^{\bullet}$ and a third one with the regeneration of the native state of the enzyme by interaction of Cpd-II with other AH molecule and the generation of a second radical $A^{\bullet}$ and water. Details of the mechanism can be found in the Dunford book and other works [41–43].

The overall reaction of hydrogen peroxide and ARS (AH) is proposed to be:

$$H_2O_2 + 2AH \rightarrow 2A^{\bullet} + 2H_2O \quad (4)$$

The step of formation of the compound I (Cpd-I) in HRP has been studied theoretically with different approaches by several authors. A commonly accepted mechanism for peroxidases is the Poulos–Kraut mechanism [44] that involves acid–base catalysis, through the highly conserved His-Arg couple in the distal side, resulting in an heterolytic cleavage of the O—O bond of hydrogen peroxide. In a recent paper, Derat et al. [45] used QM/MM calculations to describe the structure and spectroscopy of the active species Cpd-I of the enzyme horseradish peroxidase (HRP). One of the conclusions of the study was that the distal residues, His42 and Arg38 are essential and have to be included in the quantum mechanical (QM) subsystem for reproducing structural and Mössbauer spectroscopic features for this species. One key point was that for the Mössbauer parameters to be reproduced, the hydrogen bonding network leading from the oxo group of Cpd-I through the crystalline water molecule (W427) and the doubly protonated His42-H^+ must be included [40,46]. In a subsequent manuscript Derat amd Shaik [47] studied through QM/molecular mechanics (MM) the O—O bond activation in the enzyme HRP, at neutral to basic pH. Two different, alternative mechanisms for the formation of Cpd-I were analyzed. One is from the ferric—hydrogen peroxide intermediate and the other from the ferric—hydroperoxide (PorFe—OOH) or compound 0 (Cpd-0). The ferric—hydrogen peroxide complex can undergo 1,2-proton shift and heterolytic cleavage to form Cpd-I. This mechanism has been ruled out due to its high energetic barrier. A low energy mechanism can be initiated by deprotonation of hydrogen peroxide and then O—O bond heterolysis of the Cpd-0 species. His42-H^+ relays the proton to the distal oxygen of Cpd-0 and leads to simultaneous heterolytic cleavage of the O—O bond, resulting in Cpd-I and water – identified as W427. The positively charged Arg38 facilitates the heterolysis of the O—O bond.

Now, one of the controversies related to the Cpd-I formation and its interaction with H_2O_2 is what happens with the water formed. The questions that concerned us and several other authors have been:

1- Does this water molecule remain coordinated to the Fe=O of the compound I or coordinated to the His42-Arg38?
2- What is the role of this water molecule, if coordinated in the neighbourhood of the catalytic Fe=O bond, in the coordination of the phenolic aromatic substrate and the subsequent hydrogen abstraction from it?
3- What is the role of this water molecule in the formation of the Cpd-II in the case of HRP?

The controversy leads to Vidossich et al. [48] to propose two different mechanisms for the Cpd-I formation through the Cpd-0:

1- The “dry” mechanism, without water coordinated to any of the aminoacid residues near the Fe or to the Fe=O bond or the H_2O_2.
2- The “wet” mechanism, with water coordinated to Fe=O, to His42 and H_2O_2.

The authors concluded that the Cpd-0 formation in HRP (PorFe—OOH) follows the wet mechanism and the deprotonation of the distal peroxide oxygen by His42 with the concomitant breakage of the O—O bond is the rate-limiting step of the process. Moreover, there are close interactions between water molecules and peroxide in both the Fe(III)—H_2O_2 and Cpd-0.

Recent isotopic labelling study showed that HRP turnover conducted from non-labelled hydrogen peroxide and isotopically labelled water results in the isotopic enrichment of the hydrogen peroxide. This finding is difficult to explain and perhaps Cpd-I formation is not involved in the isotopic enrichment [48,49]. With this background we selected a model of HRP-Cpd-I with one water molecule coordinated to the O of the Fe=O to perform our MM2–PM6 calculations of the adsorption energy of two different substrates: (a) a second hydrogen peroxide molecule and, (b) the ARS molecule.

All the key residues for catalytic function and the aromatic substrate binding were considered in case of HRP. Two HRP models were used: large model (LM) and reduced model (RM). For the MM2 calculation the complete structure of the distal and proximal sites were included, such as all the key residues for the catalytic activity. For the PM6 (MOPAC 2009) calculation, only the Arg38, His42, His170, and the key residues for the aromatic binding were maintained. The results of the MM2 calculations for the LM and RM are included but they are only used for comparative purposes with the semiempirical results.

In the case of the hematin, we included six water molecules around the Fe=O moiety. One of these water molecules is replaced by the H_2O_2 or the ARS. In the case of ARS two different orientations were analyzed: through the hydroxyl group called 1 and through the hydroxyl group called 2. Fig. 2 shows the different models used in the MM2 and the PM6 calculations for hematin and for HRP and the relative size of substrates and catalyst models.

The MOPAC 2009 was selected as the software to perform the PM6 calculation [50,51]. Fe parameters are included in the software. The results are done in the UHF (unrestricted Hartree Fock) mode that allows the presence of non-paired electrons.

First, a MM2 calculation was performed to obtain a steric energy minimum using a Chem 3D 5.0 Ultra from Cambridge Soft, for the LM and for the RM. Later a single point calculation was done using the PM6 methodology at the minimum obtained for the RM by the MM2. The MM2 results are only included to show the trend, whereas the PM6 software provides the ΔH_r for the adsorption reaction as a difference between the ΔH_f of the final state and the initial state. The results of the reduced model are related to the same structures whose ΔH_r are obtained using PM6. The graphs of the minima found by calculation were done using ChemBio 3D Ultra 11.0.

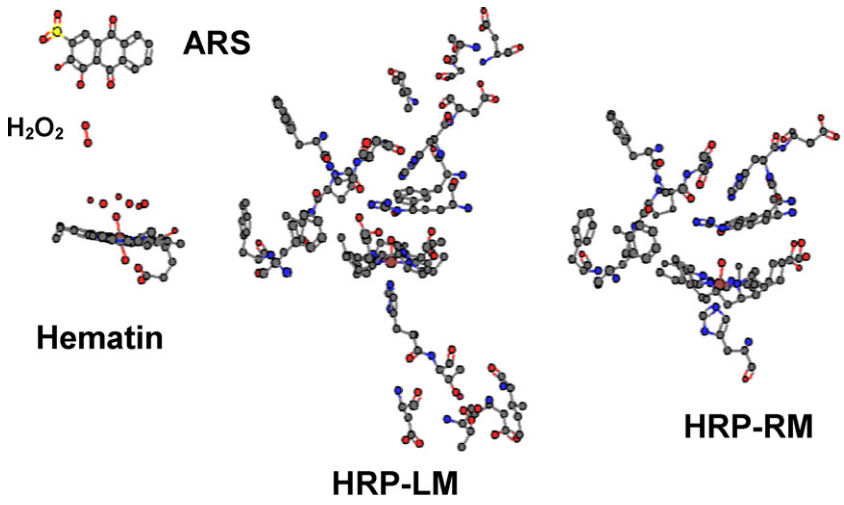

Fig. 2. MM2–PM6 models – hydrogen atoms are not shown for clarity.

The general substrate adsorption reactions considered in the MM2–PM6 for hematin and HRP are

$$\text{HematinFe=O—6H}_2\text{O} + \text{Substrate} \rightarrow \text{HematinFe=Obond—Substrate—5H}_2\text{O} + \text{H}_2\text{O} \quad (5)$$

$$\text{HRPFe=O—H}_2\text{O} + \text{Substrate} \rightarrow \text{HRPFe=Obond—Substrate—H}_2\text{O} \quad (6)$$

Substrate 1 is H_2O_2 and Substrate 2 is ARS.

3. Results and discussion

3.1. ARS solution behaviour

ARS solutions presented a turbid appearance independently of pH. Open literature reported the formation of ARS molecular aggregates. The molecular aggregates are built by stacked ARS molecules [10]. Fig. 3 shows the different anthraquinoid resonant structures of ARS at different pHs and Fig. 4 shows the influence of the pHs and catalyst on ARS solutions at different pH-values. The 420–640 nm band's shape and location of the maximum absorbance changes with the pH. The 511–520 nm band is assignable to the $n \rightarrow \pi^*$ transition of —C=O (ARS). The new shoulder at 600 nm is assigned to the conjugated carbonyl groups found at pH 10.6, related to the formation of new —C=O bonds as a product of the two —OH deprotonation at that pH (see Fig. 3, black circle at bottom). The increase of the absorbance in the pH range from 7.4 to 9 between 420 and 620 nm may be related to de-aggregation of ARS dimers/oligomers. The ARS structure changes with the pH. At pHs 7.4 and 9, more and more species with ionized OH2 (and quinoid resonant species) are present (the first p*K*a of sodic ARS is 5.5–6.7 assignable to OH2). The main species is a dianion. With a second p*K*a of 11 for sodic ARS, the relative concentration of the ARS trianion to the ARS as dianion at pH 10.6 is 0.4. At pH 10.6 an important proportion of ARS is a trianion – with the two OH ionized plus the sulfonic group as sulfonate. There is an isosbestic point in these spectra at 525 nm, confirming that there are two species coexisting at pH 10.6 [52].

Pirillo et al. [7] have observed Alizarin aggregates in aqueous solution, and Alizarin has a very similar structure to ARS. ARS dimers formation by hydrogen bonding have been studied before [53]. Aggregation is observed in UV–vis spectra as a decrease of

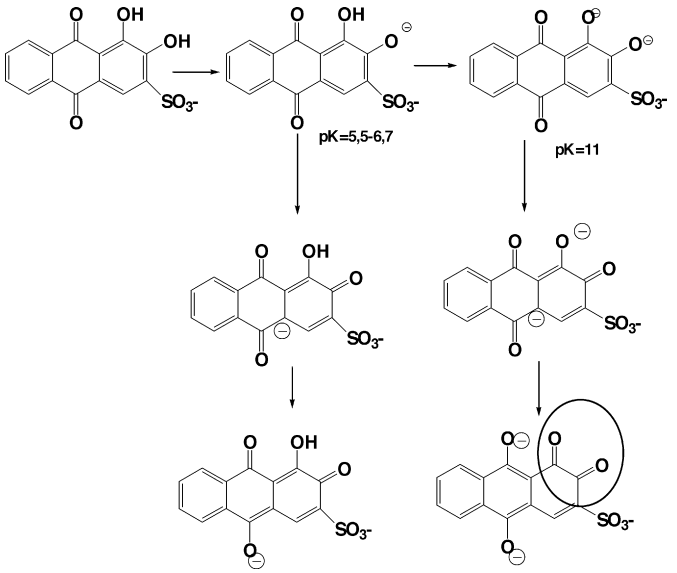

Fig. 3. Resonant structures at different pHs of ARS.

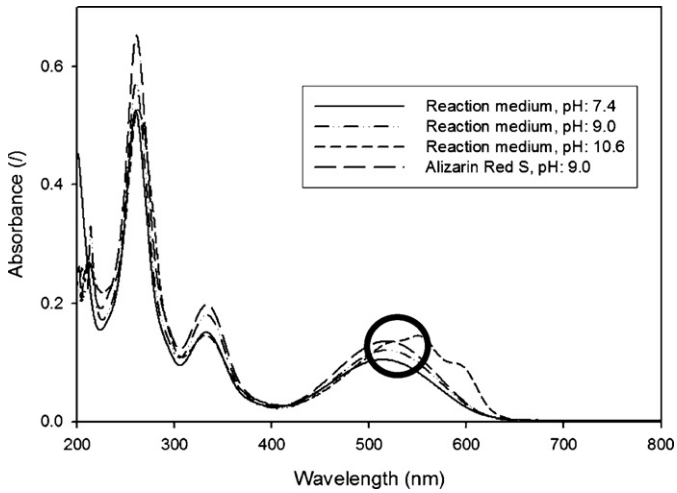

Fig. 4. Alizarin Red S spectra at different pHs in the reaction medium (buffer + catalyst). Isosbestic point marked with a circle.

Table 2
Results of conversion and catalytic yield.

Exp. no.	HRP		Hematin	
	Conversion, Y (%)	Catalytic yield, Z (g^{-1})	Conversion, Y (%)	Catalytic yield, Z (g^{-1})
1	30.5 $_{(\pm 14.6)}$[a]	1069 $_{(\pm 156)}$[a]	77.6 $_{(\pm 0.6)}$[a]	3773 $_{(\pm 58)}$[a]
2	28.0	1361	61.2	2982
3	25.9	907	71.0	2488
4	29.2	800	92.3	2527
5	57.1	12511	73.5	16106
6	21.8	763	86.4	3030
7	27.7	606	66.8	1463
8	40.5	8869	77.2	16916
9	39.5	1083	92.6	2716
10	25.5	2034	88.3	2738
11	16.0	299	72.2	2537
12	22.7	1105	61.8	3010
13	13.8	257	71.8	1339
14	19.5	301	92.3	1423
15	23.2	358	93.6	1444
16	29.8	1335	102.7	4606
17	12.9	254	91.9	1814
18	13.0	2829	23.8	5164
19	27.4	5950	17.7	3851
20	3.0	292	22.2	2171
21	0.0	0	0.0	0.0

[a] Average values of central point repetitions. The standard error (as the standard deviation/medium value) is presented in each case.

the absorption band or a batochromic shift in comparison to a monomer solution spectra [54].

3.2. ARS decolorization reactions

Table 2 shows the response values of the experimental design. To determine whether hydrogen peroxide is capable to decolorize ARS solutions by non-catalytic ways, reactions were performed without catalyst at pH 9 and 10.6 with an initial peroxide concentration of 2.5 mM. Only 2.3% and 3.4% conversions were obtained, respectively, evidencing the catalytic nature of decolorization in the presence of hematin or HRP.

3.2.1. Hematin as catalyst

The quadratic models obtained to fitting conversions (Y) and catalytic yields (Z) responses of Table 2 to Eq. (1) are (factors are represented as coded values):

$$Y = 76.6_{(\pm 0.87)} + 43.3_{(\pm 1.7)}X_{[\text{Hematin}]} + 17.6_{(\pm 1.7)}X_{\text{pH}} - 4.1_{(\pm 1.6)}X_T - 18.4_{(\pm 4.2)}X^2_{[\text{Hematin}]} - 40.34_{(\pm 9.0)}X_{[\text{Hem}]}X_{\text{pH}} \quad (7)$$

$$Z = 2080_{(\pm 424)} - 6943_{(\pm 742)}X_{[H_2O_2]} + 873_{(\pm 750)}X_{[\text{pH}]} + 8779_{(\pm 1269)}X^2_{[H_2O_2]} \quad (8)$$

The selected models represent the best relationships among the responses and the statistically significant factors. For conversion the coefficient of determination is $R^2 = 98.69\%$ and adjusted $R^2 = 98.33\%$. For catalytic yield the coefficient of determination is $R^2 = 86.43\%$ and adjusted $R^2 = 84.40\%$. The increase of hematin concentration has a positive effect on ARS conversion, such as the

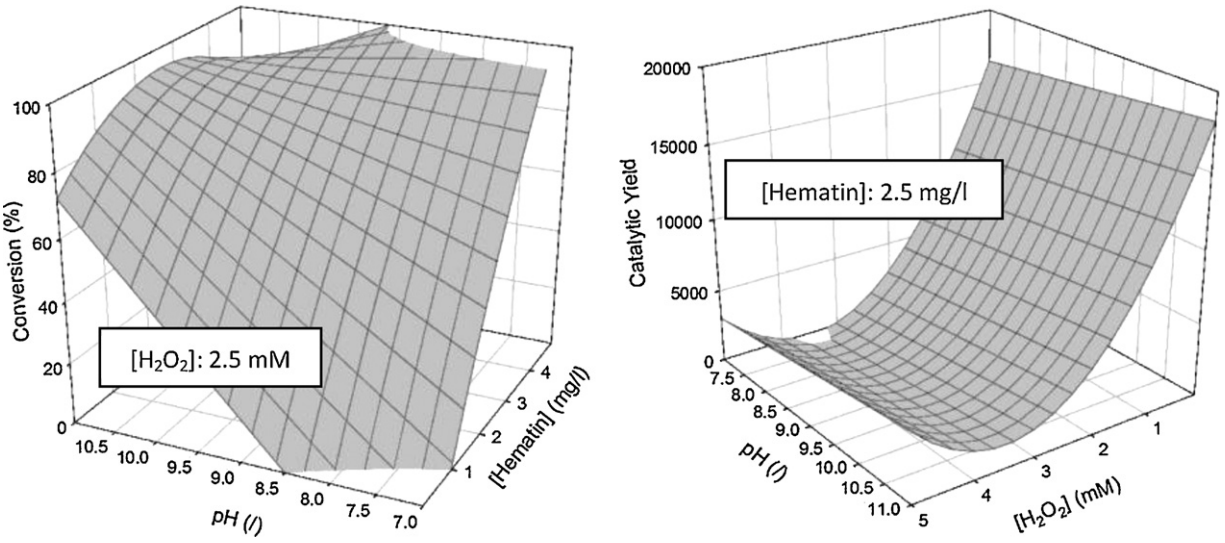

Fig. 5. Response surfaces for conversion and catalytic yield in hematin/ARS system. Temperature was fixed in 40 °C.

increase of pH from neutral to alkaline. Catalytic yield is affected by the increase of pH. On the other hand, the catalytic yield presents a minimum value at middle hydrogen peroxide concentrations, increasing afterwards (see Fig. 5). This may be associated to the production of inorganic radicals at high hydrogen peroxide concentration, which attack the ARS structure [55–57]. However, Zucca et al. [58] have demonstrated the non-participating nature of HO• radicals in ARS oxidation by a manganese porphyrin as a peroxidase-like catalyst. On the other hand, increasing yield at high peroxide concentrations may be a result of a parallel catalytic cycle involving H_2O_2 molecules that return hematin into its native state as e.g. the catalase-like activity pathway [59].

The hematin solubility in water increases with the increase of pH. Also, De Villers and coworkers have studied the catalyst behaviour in aqueous solution and demonstrated that dimerization constant has a maximum at pH = 7.5 and decreases afterwards [60]. Accordingly, the combination of alkaline pH and high hematin concentration should promote ARS conversions. Also, hydrogen peroxide (with a p*K*a = 11.62) produces a higher proportion of active hematin intermediaries by reaction of Fe^{3+} with a more easily oxidized species, HOO^- [61]. However, the conversion has a maximum at pH 10 and then it falls down. Emmert III et al. [62] studied azo-dyes oxidation by metalloporphyrins and determined that the oxidation reaction occurs by hydrogen abstraction. ARS at pH < 5.5 is present as monoanion, at 5 < pH < 11 as dianion and pH > 11 as a completely deprotoned trianion [63]. If there are no hydrogen available to react with the Fe=O bond of hematin, ARS radicals are not going to be generated. To obtain high ARS conversion, a compromise between the amount of hematin available and the ARS reactivity at pH values between 9.5 and 10 is required.

3.2.2. HRP as catalyst

Quadratic models selected to fit the studied responses with HRP as catalyst are:

$$Y = 29.2_{(\pm 1.5)} + 13.5_{(\pm 3.1)}X_{[H_2O_2]} + 6.5_{(\pm 3.1)}X_{[HRP]} + 3.8_{(\pm 3.1)}X_T - 51.4_{(\pm 10.1)}X_{[HRP]}X_{pH} - 13.0_{(\pm 7.8)}X_{[H_2O_2]}X_T + 11.9_{(\pm 8.9)}X_{pH}X_T \quad (9)$$

$$Z = 725_{(\pm 350)} - 4627_{(\pm 645)}X_{[H_2O_2]} - 1083_{(\pm 638)}X_{[HRP]} + 6153_{(\pm 1107)}X^2_{[H_2O_2]} + 4398_{(\pm 1863)}X_{[H_2O_2]}X_{[HRP]} \quad (10)$$

These models have low coefficients of correlation. For conversion R^2 = 74.04% and adjusted R^2 = 65.84% and for catalytic yield, R^2 = 79.48% and adjusted R^2 = 75.58%. Compared to hematin, HRP catalyzed ARS decolorization results are different (see Table 2 and Fig. 6). The goodness of fit just explains the 74.03% of the experimental results.

The hydrogen peroxide concentration has an important negative effect on conversion. HRP suffers inactivation by excess of H_2O_2 and by organic radical attack to aminoacidic residues. H_2O_2 inactivation is produced by an alternative reaction pathway of Cpd-I [42] whereas the second mentioned inactivation pathway may involve ARS radicals formed during the catalytic cycle [64–66]. Alizarin has a similar structure to ARS but this behaviour was absent in previous studies from our research group [7], where high conversions were found even at high hydrogen peroxide concentration. It is more reasonable to think that ARS is not a good substrate to HRP due to its volume and the presence of the sulfonic species as an important difference with Alizarin or in a secondary reaction different in the case of Alizarin vs. ARS.

The pH does not affect the studied responses. A negative interaction between pH and HRP concentration exists. This is consistent with reported HRP catalytic activity for simple substrates which is

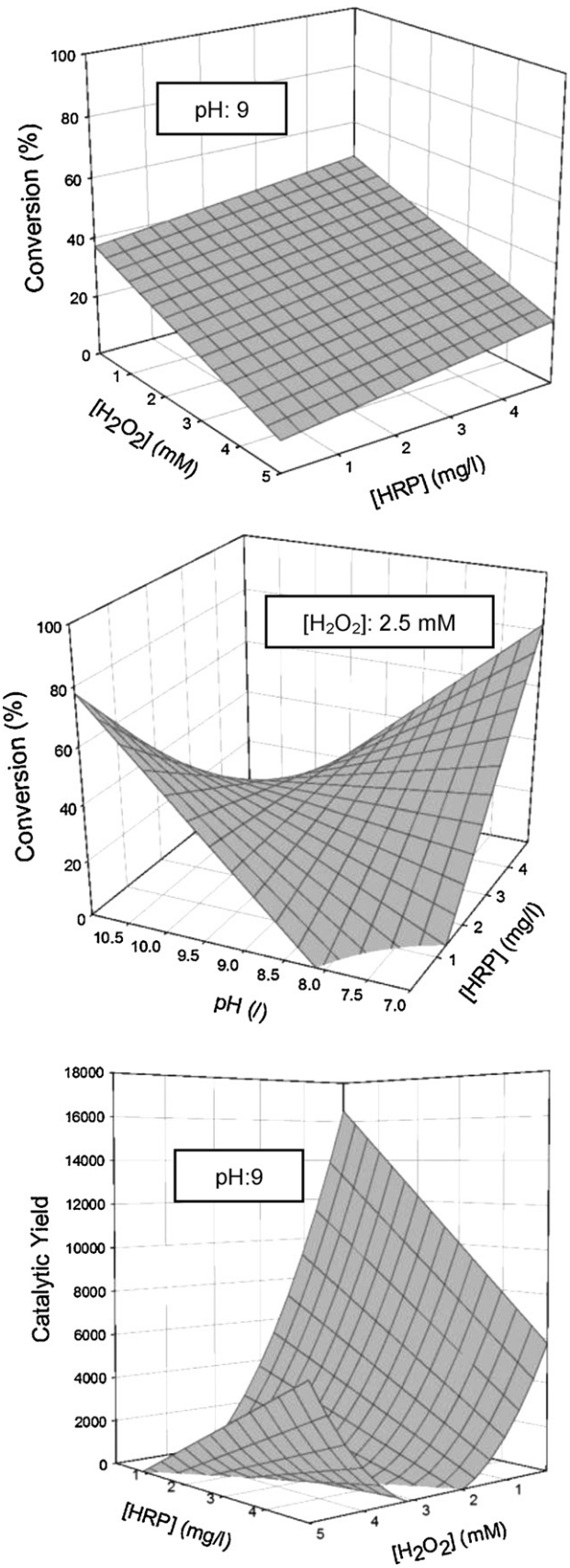

Fig. 6. Response surfaces for conversion and catalytic yield in HRP/ARS system. Temperature was fixed in 40 °C.

almost constant in the pH range from 7 to 9, falling down at higher pH values [42]. Also, the increase of ARS deprotoned molecules at pH near 11 does not permit the radical formation by hydrogen abstraction.

Catalytic yield decreases with the increase of hydrogen peroxide concentration probably due to H_2O_2-induced inactivation (suicide inactivation). Moreover, the yield increases at high HRP and H_2O_2 concentrations (see Fig. 6), being this finding consistent with a lower H_2O_2 inactivation effect since more enzyme is available. This behaviour may also be associated to an increase of the relative concentration of HRP native state by the catalase-like pathway [59]. However, no important amounts of released oxygen are found with this catalyst (see Section 3.4) at our experimental conditions.

3.2.3. Desirability function

Considering that the responses of catalytic yield and conversion are correlated, a desirability function (DF) is included. Fig. 7 shows the results of DF for the hematin Cpd-I and HRP Cpd-I. Optimal balances between the conversion and the yield per mg of catalyst and per milimol of oxidant are desirable. The Derringer function or desirability function [67] is the most used. The scale of the desirability function goes between $d = 0$ and $d = 1$. Despite the obvious advantages of the Derringer function, unfortunately there are very few applications found in the literature in engineering applications [68].

It is evident that HRP is very sensitive to the increase of the H_2O_2 concentration and never reaches the value 1. The optimal value for the desirability function is found at the lowest range of the H_2O_2 concentration and the middle HRP concentration. The increase of HRP concentration does not help to increase the desirability function. This finding implies that something is affecting the availability of the enzyme to the substrate. This may be the aggregation of HRP. Aggregation of proteins/enzymes in buffered aqueous solution is an important problem that many times is not properly addressed when free enzymes are tested in aqueous systems [69].

For HRP the desirability function is proposed to be the result of four different reactions going in parallel: the generation of inorganic/organic radicals at high levels (at high HRP concentrations and related to higher conversions), the destruction of the heme and/or proteic structure of HRP (at high H_2O_2 concentration) plus the aggregation of HRP (at high HRP concentration) and finally the potential negative impact of dimers/oligomers of substrate in the inhibition of HRP (highest at the lowest HRP concentration and highest H_2O_2 concentration). The blocking of HRP has been reported as inhibitory with certain substrate structures [70]. Three of these reactions decrease the final ARS conversion.

The problem of protein aggregation or the blocking of the enzyme active site by dimeric ARS in HRP is not present in the case of hematin. Best results for the combined analysis of ARS conversion and catalytic yield are found at the highest hematin concentration and the middle concentration of H_2O_2 of the whole range studied. However, increasing the hydrogen peroxide concentration, the partial degradation of the porphyrinic ring due to the high amount of inorganic–organic radicals generated is the probable cause of the decrease of the desirability function to values lower than 1. It seems that in the case of hematin the desirability function is the result of two different reactions going in parallel: the generation of inorganic/organic radicals at high levels (at high hematin concentration) plus the destruction of the heme structure of hematin (at high H_2O_2 concentration).

3.3. UV–visible decolorization analysis

Fig. 8 shows the UV–visible spectra for ARS solutions, before and after treatment, with HRP and hematin as catalysts at selected conditions. The decolorization is more effective with hematin/H_2O_2. However, with both catalysts the drop of the absorbance at characteristics wavelengths is evident. Between 200 and 220 nm an increase of absorbance is related to the formation of aromatic compounds with smaller molecular weight than ARS and high absortivity ε. These characteristics permit us to postulate the degradative nature of oxidation mechanisms of ARS with HRP and hematin at the selected range of conditions here studied. The presence of sulfonic group in the dye structure affects the degradative mechanism due to its great volume and net negative charge. Degradative mechanisms with diquinone formation in ARS decolorization have been proposed with lacasse and 5,10,15,20-tetrakis(4-sulfonatophenyl)porphine–Mn(III) as catalysts by Zucca et al. [58]. Also, degradative pathways of ARS solutions treated with photo Fenton, electro Fenton, electrochemical or photocatalytic process have been observed [5,71–74].

3.4. Profiles of reaction at selected conditions

Fig. 9 shows oxygen, hydrogen peroxide and ARS concentration profiles with reaction time at selected conditions. The study of consumption or release of oxygen and hydrogen peroxide with ARS oxidation may give insight into the differences in the reaction pathways with both catalysts.

The ARS concentration only decreases 40% of the initial value with HRP as catalyst. Besides, the hydrogen peroxide consumption and dissolved oxygen are almost invariable after the first 20 min. No clear catalatic reaction is taking place.

In case of hematin/H_2O_2 system, the results are very promising. The ARS concentration decreased almost to zero. Hydrogen peroxide concentration decreases and dissolved oxygen concentration increases. This is assignable to catalatic activity of hematin. A mechanism of radicals generation catalyzed by hematin has been proposed by Akkara et al. [75] for ethyl phenol polymerization. The reactions and intermediates involved are proposed to be similar to those found in the HRP mechanism. That proposed mechanism [75] is associated to a higher consumption of H_2O_2 for hematin vs. HRP and is in agreement with our results.

The mechanism of reaction of hematin with H_2O_2 needs the sixth coordination position of Fe of hematin to be occupied by H_2O_2 (Cpd-0) before the formation of Cpd-I. The increase of H_2O_2 consumption and O_2 production in the beginning of the reaction is noticeable with hematin in Fig. 9. Stephenson and Bell [76,77] have proposed a mechanism with a Fe(III) porphyrin which involves a homolytic and a heterolytic rupture in parallel with a compound-0 previous formation. The homolytic pathway results in the formation of a higher relative amount of inorganic radicals than the heterolytic one. Moreover, they observed that heterolytic cleavage is faster that homolytic in protic solvents, pointing to a role of protons in the mechanism. On the other hand, the release of oxygen during the reaction is different from the release of oxygen obtained with the similar structure alizarin and in the oxidation of other dyes like Eriochrome Blue Black and Fluoresceine using hematin, but at different H_2O_2 concentration (21 mM) and at pH 7 [7,78]. Granados-Oliveros et al. [55–57] have studied the formation of inorganic radicals and their effect on organic compounds oxidation. These studies have concluded that in presence of methalloporphyrins the principal radical formed is $O_2^{\bullet -}$ with H_2O_2 (10–100 mM). This species is a principal precursor to $HO^{\bullet}$ formation ($O_2^{\bullet -} + H_2O_2 \rightarrow HO^{\bullet} + OH^- + O_2$). In this framework, there is an initial consumption of O_2 and a posterior production.

We propose the peroxidase-like mechanism with a heterolytic cleavage of O—O bond as the most important reaction pathway for the ARS oxidation using hematin or HRP biocatalysts in presence of hydrogen peroxide.

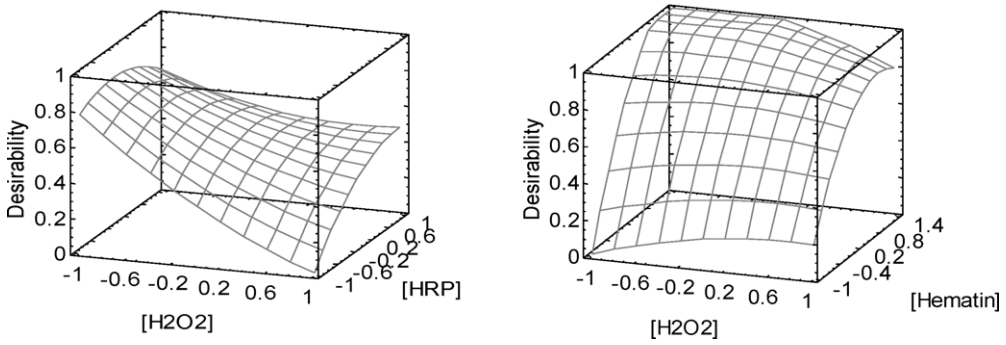

Fig. 7. Desirability functions for hematin and HRP, considering catalytic yield and ARS conversion. Independent variables are coded, pH: 9.0; *T*: 40 °C.

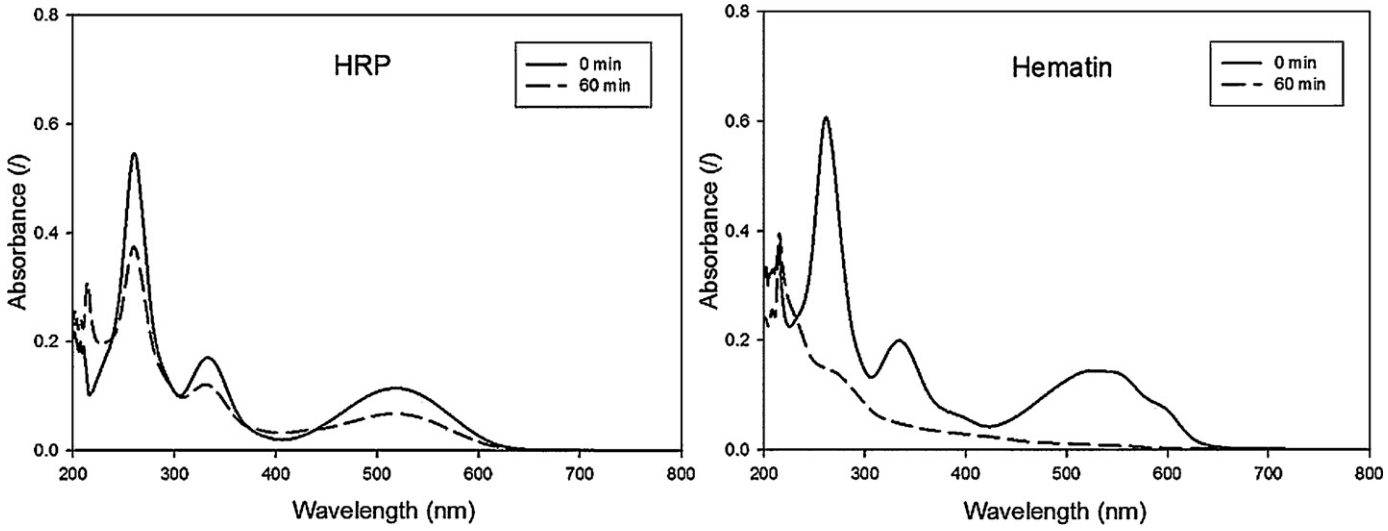

Fig. 8. UV–vis spectra of ARS 75 mg/l solutions, at initial time and after treatment. HRP system: [HRP]: 2.5 mg/l; [H_2O_2]: 0.4 mM; pH: 9; *T*: 35 °C. Hematin system: [hematin]: 4.44 mg/l; [H_2O_2]: 3.2 mM; pH: 9.4; *T*: 45 °C.

3.5. UV/visible spectra of HRP–H_2O_2 and hematin–H_2O_2 at different H_2O_2 concentrations

UV/visible spectra for HRP and hematin with different concentrations of H_2O_2 at pH 10 are shown in Fig. 10. First, there is a clear difference in the values of absorbance obtained for hematin vs. HRP, being lower for HRP. Low absorbance values are characteristic of aggregates [69]. This is a sign of aggregation in the case of HRP. Aggregation does not affect enzymatic reaction with H_2O_2, because hydrogen peroxide is a small molecule. The presence of buffer and

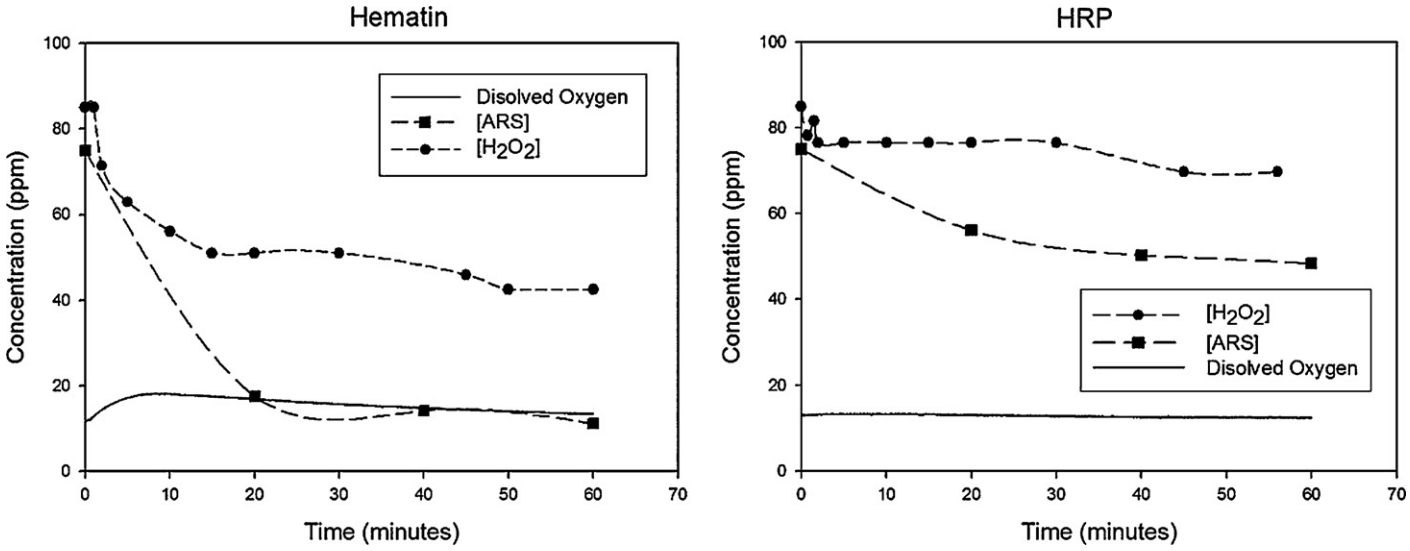

Fig. 9. Profiles of dissolved oxygen, ARS and H_2O_2 concentration. Initial conditions: [H_2O_2] = 2.5 mM, [ARS] = 75 mg/l, pH = 9, *T* = 30 °C, [HRP] = 4 mg/l, [hematin] = 4 mg/l.

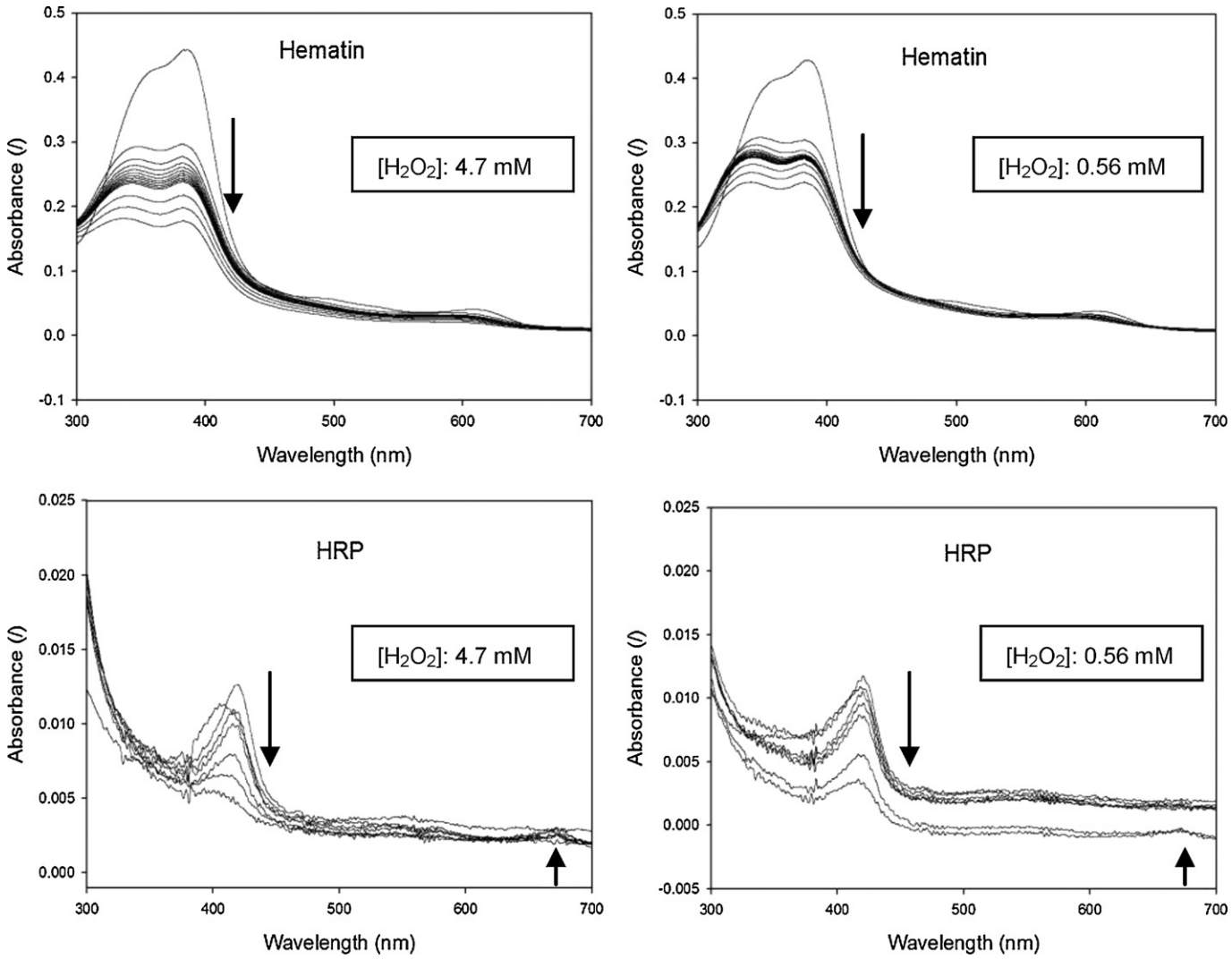

Fig. 10. UV/visible spectra of hematin–HRP with H_2O_2 at the highest and lowest concentrations included in the Doehlert design. Initial conditions: pH = 10, T = 30 °C, [hematin] = 5 mg/l, [HRP] = 5 mg/l. With hematin [buffer] = 0.1 M; with HRP [buffer] = 0.01 M.

the high concentration of HRP increase aggregation (results not shown).

There is an interesting trend at first sight in these figures for HRP and hematin. At the lower concentration of H_2O_2, with hematin the band near 350 nm has a different absorbance than that of 395–400 nm, whereas at the higher concentration the importance is similar. It seems that two reaction phases are present: a first one where an important decrease is present and later an increase to a final species that remains stable.

There are three bands assigned to electronic transitions $\pi \rightarrow \pi^*$ in metalloporphyrins: α, β (Q bands), and γ (or B-Soret). The α transition originates from 3a2u ($\pi-$) and the final state is 4eg ($\pi-^*$). The β band has the same origin but the final state is an excited level 4eg (π^*). The Soret band is from the basal 1a1u (π). In the case of Fe d^5 there are additional bands provided by electronic transitions from the occupied orbitals of higher energy of porphyrin to the unoccupied states of lower energy of Fe (transitions from 3a2u (π) of porphyrin to e.g. ($d\pi$) of Fe) or charge-transfer (CT) bands. The Soret bands are located in 380–420 nm whereas the Q bands are present between 500 and 650 nm [42,79]. The Cpd-I of peroxidase shows an important decrease of the intensity of 403 nm band due to changes in ε (from 102 to $53.8 \times 10^{-3}\,M^{-1}\,cm^{-1}$), whereas the shoulder at 380 nm is lost. There are also two bands at 495–500 nm and 641–650 nm [80]. Cpd-II presents a Soret band at 420 nm of high ε ($105 \times 10^{-3}\,M^{-1}\,cm^{-1}$) and a doublet at 527–555 nm. Charge-transfer bands disappear in low-spin complexes with OH^- or CN^- as ligands [42,81]. Compound-III is a complex ferric superoxide that exists as ionic-pair and presents a Soret band at 417 nm, with other Q bands at 580 and 544 nm [42].

The interaction of hematin with H_2O_2 generates compound-I, such as it also does in the case of HRP. The decrease of the 395 nm and of the 370 nm shoulder is evident at both concentrations. The absorbance decrease of the 370 nm band to near 345–350 nm is also noticeable and higher as expected using the higher peroxide concentration. It seems that there are two steps of reaction: first an important decrease of the absorbance of this band and after a short increase until a stable situation is achieved. Using the higher hydrogen peroxide concentration, bands at 395 nm and 345–350 nm are similar in absorbance, whereas the one at 345–350 nm is higher in relative importance using lower hydrogen peroxide concentration. The band at 372 nm has been assigned to ferric ion and may be used to check for the formation of Cpd-I. On time on reaction, an inactive form of hematin is generated. Being only peroxide present, there are two main routes for hematin in the reaction with hydrogen peroxide, the catalatic pathway with Cpd-I as intermediary and the inactivation by reaction of the porphyrinic moiety with H_2O_2

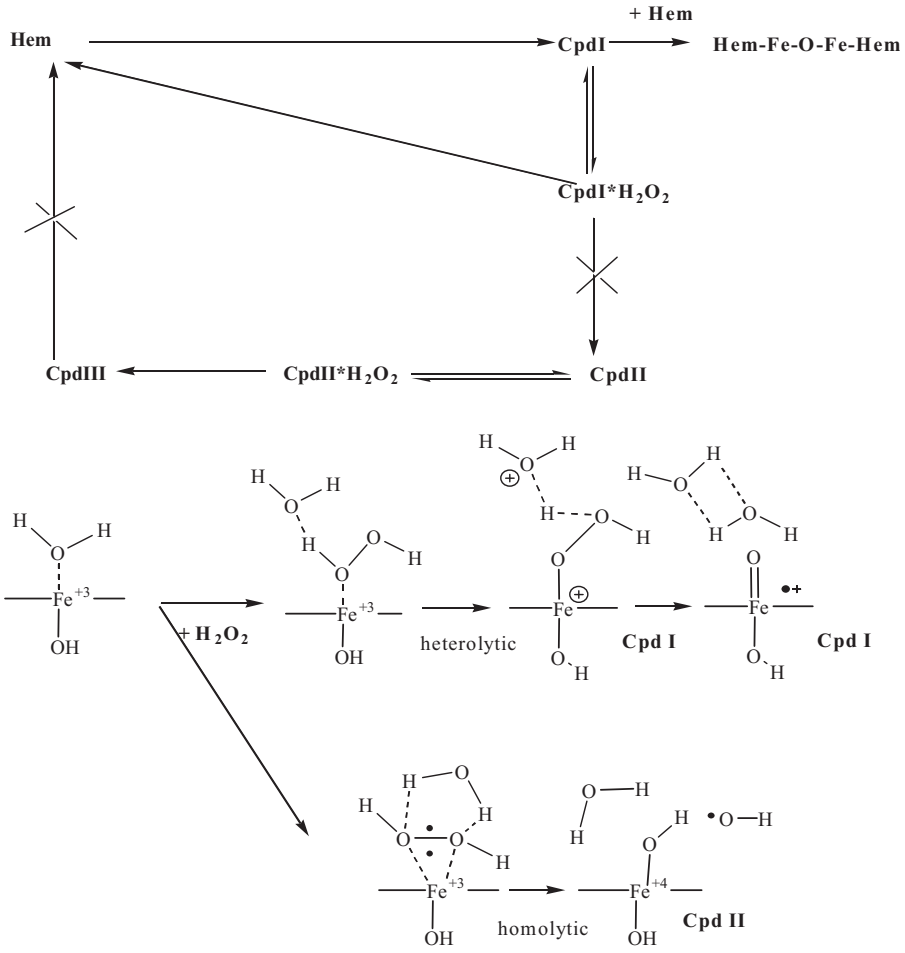

Scheme 1. Different species found in iron porphyrin/H_2O_2 systems.

through organic oxidation. However, the possibility of hematin dimer formation should also take into account, as a secondary reaction of Cpd-I:

$$Hem^{\bullet}—Fe^{+}=O + Hem—Fe \rightarrow Hem—Fe—O—Fe—Hem \quad (11)$$

Other dimer could be formed by reaction of a lateral ionized $—COO^{-}$ group of one hematin with the Fe^{3+} of other hematin, a reaction that has been published as probable [82]. This possibility is not supported by the results of the desirability function, where a clear negative impact of high hydrogen peroxide concentration is shown in Fig. 7 for hematin. With more hydrogen peroxide available, more Cpd-I is formed (more catalytic cycles are possible) – and therefore more dimerization is possible. The combined impact of high concentration of hematin and H_2O_2 favours both kinds of dimerization reactions.

Scheme 1 shows the different species proposed to be present with hematin as catalyst of hydrogen peroxide decomposition, and also includes a role of a water molecule in the formation of the Cpd-I/Cpd-II in aqueous solution. The heterolytic pathway for hydrogen peroxide reaction generates Cpd-I of hematin, whereas the homolytic pathway would produce Cpd-II. Since there is no evidence of Cpd-II in the UV/visible study of hematin–hydrogen peroxide we can discard the homolytic pathway of hydrogen peroxide decomposition. Following this idea, the formation of Cpd-II/Cpd-III with hematin is not supported in our conditions by the UV/visible study. This pathway has been explored also for epoxidation of olefins using metalloporphyrins [77].

The profile of the reaction of HRP with peroxide shows also the formation of Cpd-I, but in this case there is a shift from near 403 nm to 419 nm with time on reaction. Some partial HRP disaggregation due to interaction with the hydrogen peroxide takes place, and this is the reason of an initial increase of the band at near 400–420 nm, with later a continuous decrease. This could be assignable to the accumulation of Cpd-III (with the characteristic bands at 417 and 544–580 nm). Finally, the generation of verdoheme species (P-670) at long reaction time seems evident, with the increase of the 670 nm band and the decrease and shift to near 400 nm of the former 420 nm band.

Scheme 2 presents the main species present during the interaction of HRP with hydrogen peroxide at the selected conditions. These species are proposed with the consideration of the findings here analyzed and the results published in the open literature [59].

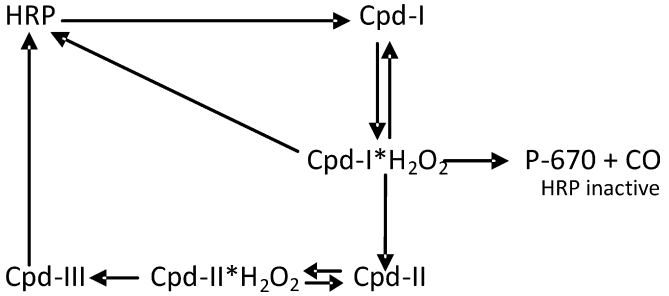

Scheme 2. Different species found in presence of hydrogen peroxide – only species of HRP are included, not hydrogen peroxide or products of each step.

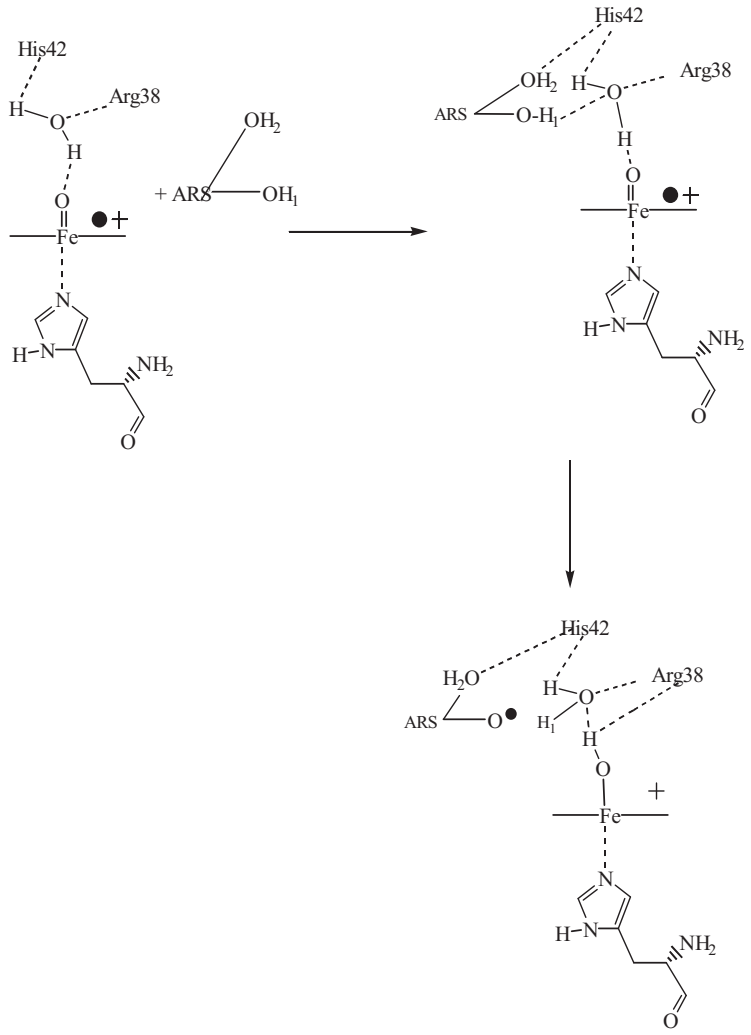

Fig. 11. Mechanism of ARS coordination and reaction with a water molecule coordinated to oxygen in Fe=O from Cpd-I/HRP.

3.6. Results of the MM2–PM6 molecular modelling

We explored the adsorption of two substrates (hydrogen peroxide and ARS) onto Cpd-I of HRP and hematin. The study of this step may give insight on the mechanistic differences between hematin and HRP when hydrogen peroxide or ARS are used.

Fig. 11 shows the proposed mechanism of Cpd-I of HRP (with a water coordinated to the Fe=O). Fig. 12 shows the result for ARS using the HRP-RM. ARS was studied coordinated with the aromatic portion in contact with the aromatic binding site of the HRP (Form 1) or with the sulfonic anionic residue pointing to the aromatic binding site (Form 2). The figure shows the aromatic binding pocket of the HRP and how the ARS locates there in two different forms. Fig. 13 shows the conformations for hematin and H_2O_2 and the two coordinations to Fe=O found for ARS in hematin. Hematin has six water molecules near Fe=O as the initial situation. Results shown are those of the minima reported in Table 3.

Coordination of a H_2O_2 molecule to the Cpd-I of HRP is endothermic (see the PM6 result for RM in Table 3). Coordination of the ARS to Cpd-I is always very exothermic. With water coordinated to the O of the Fe=O, the preferred substrate is ARS for HRP, whereas hematin may coordinate either hydrogen peroxide or ARS-1 with similar adsorption enthalpy. The coordination of the hydroxyl with the ARS coordinated to hematin in "perpendicular" form-through the OH called 2 is enthalpically favoured by near 13 kcal/mol. The results of MM2 are different, because the steric interaction is not so important in the case of ARS-1 vs. the ARS-2 coordination to hematin.

Table 3
Results in kcal/mol of the MM2 minimization (steric energy difference associated to reaction 1 or reaction 2 or ΔS_E) and PM6 single point calculation (ΔH_r).

Substrate	Hematin/Cpd-I		HRP model/Cpd-I			
	MM2 ΔS_E kcal/mol	PM6 ΔH_r kcal/mol	MM2 ΔS_E, kcal/mol			PM6 ΔH_r kcal/mol RM
				LM	RM	
R_1 H_2O_2	−12	−24	H_2O_2	−21	−24	+15.8
R_2 ARS-1	−37	−25 (OH1)	ARS-1	−29	−44	−55
R_2 ARS-2	−26	−38 (OH2)	ARS-2	−47	−50	−68

$\Delta H_r = \Sigma\Delta H_{fP} - \Sigma\Delta H_{fR}$, being P products and R reactives. LM = large model, RM = reduced model, R_1 = reaction 1, R_2 = reaction 2, ARS-1 and ARS-2 coordinations of ARS to hematin; ARS Form 1 and ARS Form 2 coordinations of ARS to HRP. There is a clear selectivity of the HRP to coordinate ARS vs. H_2O_2.

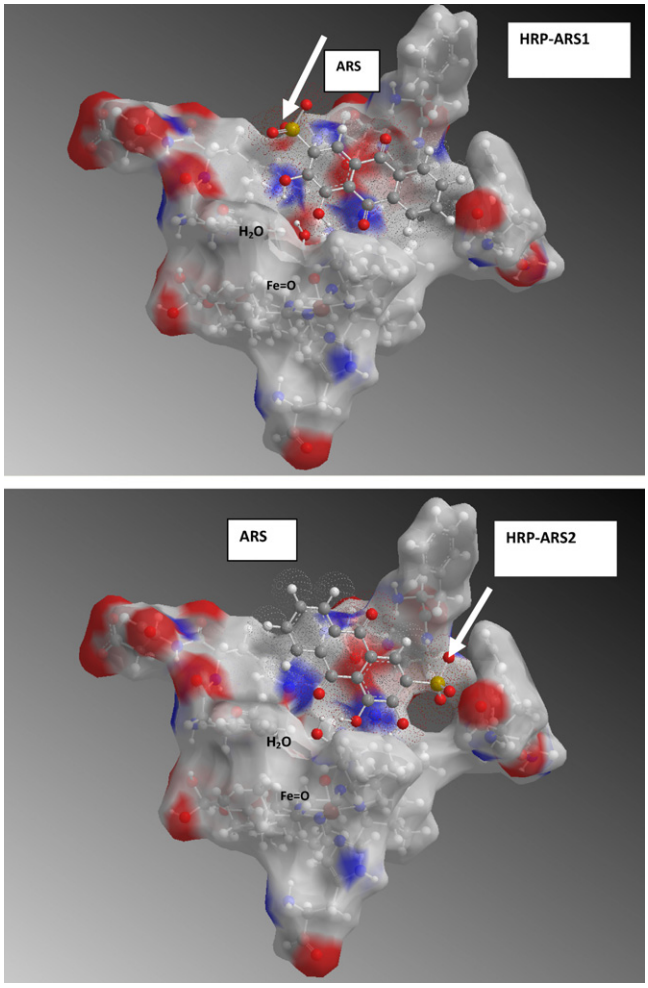

Fig. 12. Coordination of ARS in the aromatic binding pocket of HRP. The arrows point to the sulfonic group of the ARS Form 1 and ARS Form 2 (notice the sulfonic group).

Fig. 14 shows the close contacts between the water initially coordinated to the Fe=O, the Arg38 and His42 in HRP. Both conformations – Form 1 and Form 2 – showed short H-bonding between the ARS and key residues in the HRP model. If the water molecule is conserved from the Cpd-I formation coordinated to the Fe=O, it is clear that the approach of the ARS is somehow related to how this water molecule may be displaced from this position. Other aspect to consider is how this water molecule may function in the catalytic cycle to produce the Fe=O protonation. The lengths among ARS, H_2O and HRP residues are all in the range of H-bonding. The O of the water molecule coordinated to O from Fe=O is located at H-bonding length of OH1 in both coordinations. The two forms of ARS are favoured in the case of ARS-HRP RM but the coordination in the Form 2 is enthalpically favoured. From the distances found, it seems that the OH2 interaction with Arg38 is better for ARS coordination than the OH2 coordination to His42. The distances from

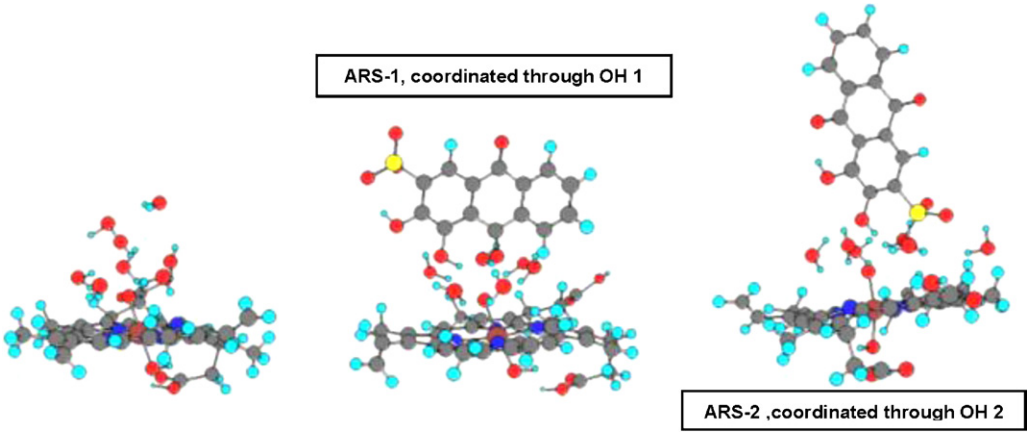

Fig. 13. Structures obtained at the minima steric energy reported in Table 3 for hematin, H_2O_2 or ARS-1 and ARS-2 coordination. See Fig. 1 for OH1 and OH2 location in ARS.

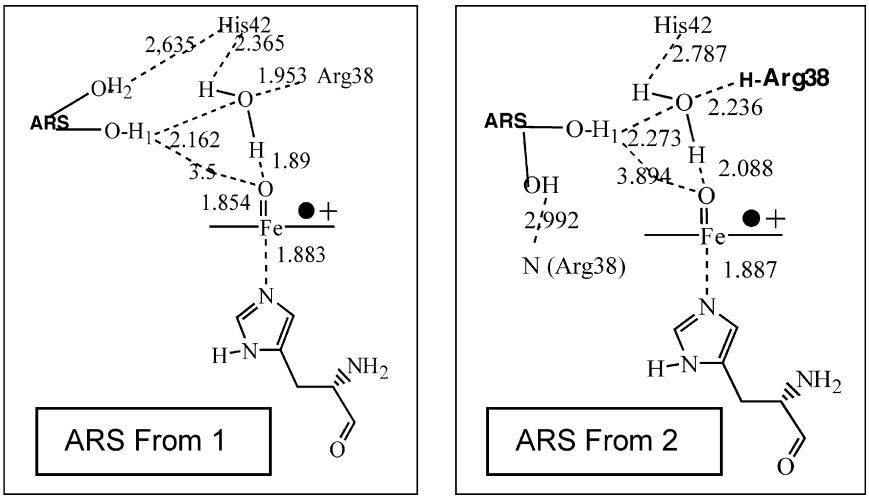

Fig. 14. ARS interactions in the Form 1 and Form 2 with key residues of HRP.

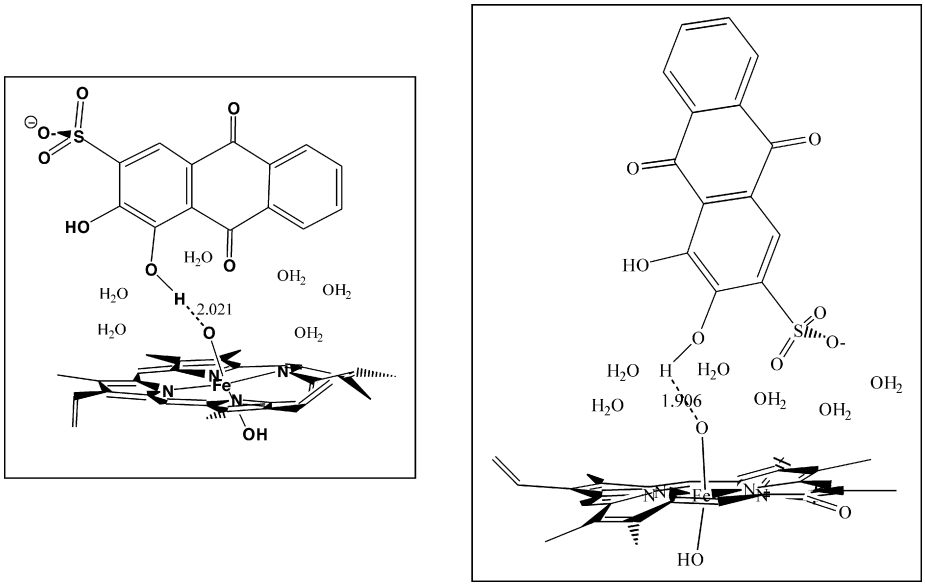

Fig. 15. ARS-1 and ARS-2 coordination to hematin.

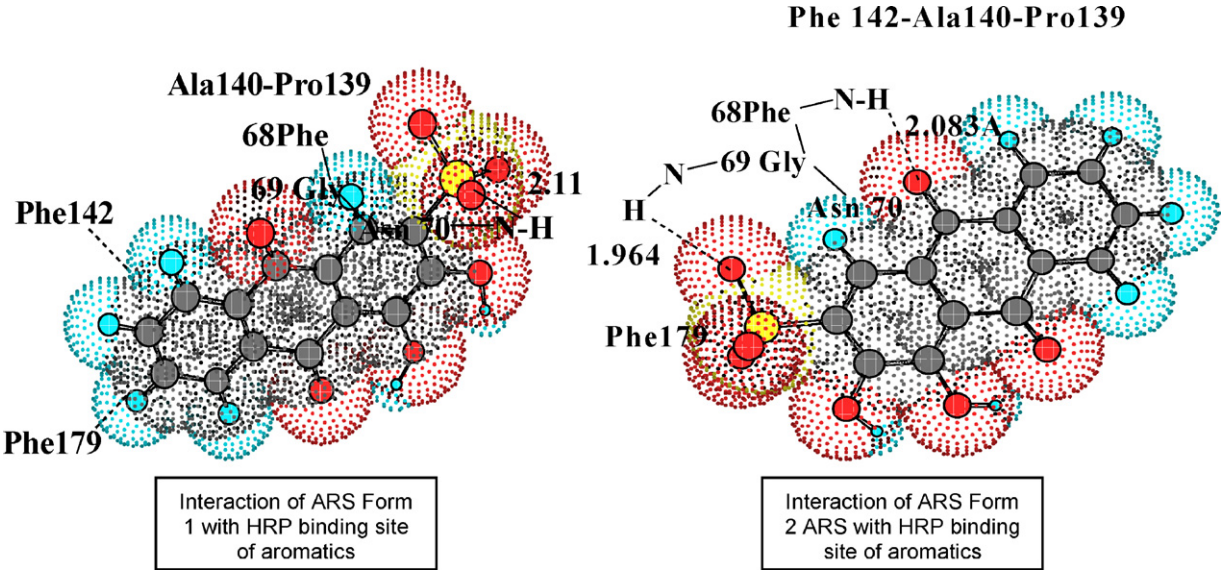

Fig. 16. ARS interaction with key binding site residues of RM HRP model.

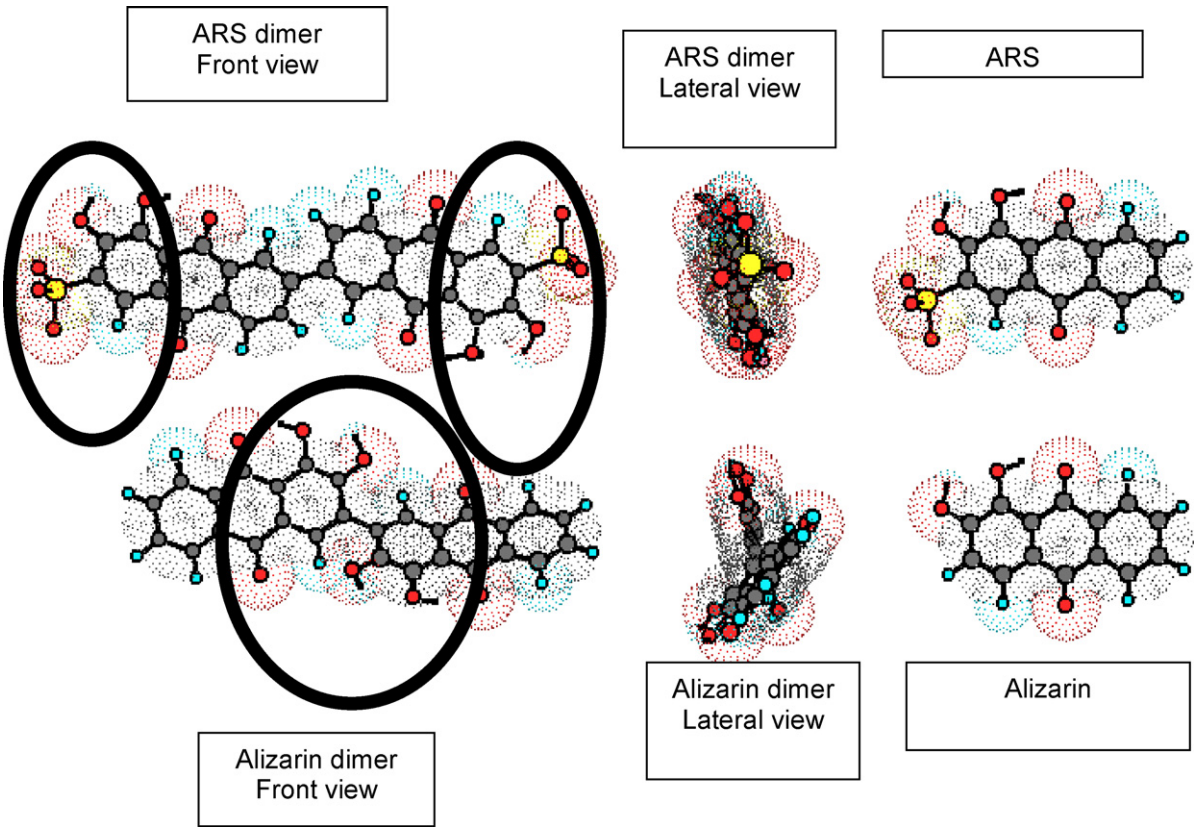

Fig. 17. Alizarin and ARS dimers.

hydrogen of water to the O of the Fe=O moiety are shorter than 2.1 A in both forms (Form 1 and Form 2).

Fig. 15 shows the H-bonding lengths found for the ARS-1 and ARS-2 coordinated to hematin. The ARS displaces a water molecule, initially located on the O of the Fe=O. Distances H(ARS)—-O (Fe=O) are 2.02 A for ARS-1 and 1.9 A for ARS-2, whereas they are in the range from 3.5 to 4 A in the case of the RM of HRP Cpd-I. At alkaline pH, the main form would be the ARS-1 due to the ionization of OH2.

Aromatic substrate binding key residues in HRP were conserved in our calculation. These residues provide a set of hydrophobic moieties that participate in the coordination of aromatics in the proper conformation for the H^+ transfer to be productive. Fig. 16 shows the distances found for the Form 1 and the residues of the aromatic binding site. The phenyl moieties of Phe are particularly important because they provide a hydrophobic channel where the aromatic phenyl groups are stabilized. However, the H-bonding interactions are also operative.

In the Form 1 the hydrophobic interactions Ph—Ph are important between the ARS and the Phe179, Phe142 and Phe68. The NH of Asn70 interacts with the ionized sulfonic group. This interaction is absent in Alizarin – that lacks the sulfonic group that ARS has. The string Phe142 with Ala140-Pro139 generates a kind of "wall" behind the ARS, whereas Phe179 is other hydrophobic moiety near the sulfonic group. Distances NH—O (ARS) and NH—O (sulfonic) near 2 A were found, clearly showing H-bonding stabilization due to interactions between HRP residues with ARS.

Structures of Alizarin (or Alizarin Red – without sulfonic group, from here thereafter it will be called Alizarin to avoid confusion) and ARS and their main dimers are shown in Fig. 17. Most favoured dimeric conformation was found by minimization and the reported one is the best structure from several explored (results not shown) or the one which provided the least steric energy as the output and/or the lower ΔH_f. In the case of alizarin, it is known that bializarin is produced when HRP is the catalyst at selected conditions [83].

From the analysis of the structures it is evident that the hydroxyls groups in ARS are located in the extremes of the molecule (see front view, black circles) whereas in the case of Alizarin they are located in the middle of the dimer (see black circle). From the point of view of the HRP and its aromatic binding pocket, this is steric and electronically very important. We will explain further why.

The aromatic substrate binding site is prepared to accommodate aromatic species, with strong hydrophobic interactions by the Phe179-Phe142 side. Alizarin and ARS may forms dimers, such as many xantene dyes [84]. Now, when the dimer of Alizarin is analyzed, the phenyl moieties are located in the extremes and the hydroxyls in the middle of the structure, able to interact with the Fe=O—H_2O. By the other side, ARS presents in the most favourable dimer found by MM2 minimization, two negatively charged species that produce repulsive interactions in the "extremes" of the dimer. These charges are near the hydroxyls groups in the ARS dimer. In the case of the ARS monomer, the binding site accommodates the sulfonic group, but in the case of the dimer, the steric and electronic interactions do not favour coordination. The charged sulfonic moiety may interact with polar group through H-bonding or even with positive charges of key residues of HRP during the reaction (charged iron or perhaps $HisNH^+$ or $ArgNH_2{}^+$?), making more difficult the proper coordination of the ARS for the proton transfer to Cpd-I and ARS radical generation.

We consider that these theoretical results may be applied to explain the different results obtained with Alizarin [7] vs. ARS using HRP/H_2O_2. The easy blocking of the HRP due to the generation of dimers of ARS is an additional problem when ARS is treated with HRP/H_2O_2. Partially, we think that this is the reason of the low conversion of ARS found with HRP in our work – with a maximum of near 57% conversion of 75 mg/L ARS at 45 °C, pH 10.6, 2.5 mg HRP/L

and 0.0032 M H_2O_2 whereas conversion of 100 mg/L of Alizarin at 45 °C is 90% at pH 7, 25 mg HRP/L and 0.021 M H_2O_2. This ARS dimer blocking may be delayed at higher temperatures because of higher rate of ARS degradation at higher temperatures and lower relative probability of ARS dimers formation.

One aspect to emphasize is that substrate coordination and H-bonding to Fe=O is direct and strong in hematin Cpd-I. Considering our modelling of HRP it seems that, following the Koulos Prater mechanism and maintaining the water molecule coordinated to the Fe=O in the Cpd-I, the H transfer from ARS to the O of Fe=O takes place through a water molecule coordinated to Fe=O. This water molecule is crucial to proton transfer, allowing the reaction of bulky substrates with Cpd-I. Our work may be the first step of a more profound and careful study on the role of this water molecule in HRP (or other similar peroxidases) mechanism. Besides, the structure of the aromatic binding site and the presence of His42 and Arg38 conditionate the reactivity of bulky molecules that may produce at low temperatures or low catalyst/H_2O_2 and high substrate concentration bulky dimers, sterically hindered to react and with inhibitory properties. Moreover, some particular structures are inhibitory because of the nature of substituents in the original molecule or the resulting structure from radical dimerization.

To the questions formerly presented the answers we propose are

1- A water molecule remains coordinated to the Fe=O of the Cpd-I of the HRP and also to the His42-Arg38.
2- This water molecule, coordinated in the neighbourhood of the catalytic Fe=O bond, is crucial in the coordination of the phenolic aromatic substrate ARS to HRP. In the case of HRP Cpd-I modelled as the HRP-RM, it is part of an H-network that participates in a proton donation from the ARS to the O of Fe=O. The role of water is particularly important for hindered or bulky aromatic phenols.
3- This water molecule is key in the formation of the Cpd-II-HRP. It is part of an H-bonded network near the Cpd-I adsorbing ARS for hematin.

4. Conclusions

In the present manuscript, the Doehlert optimization as well as the combined measurement of the hydrogen peroxide, oxygen and ARS concentrations at selected conditions, allow us to postulate some answers to several important questions. The steric and electronic structure of HRP makes this enzyme not suitable for the degradation of certain kind of dyes, such as ARS, even when it is very efficient in the degradation of a familiar structure, like Alizarin. This finding emphasizes the substrate specificity of the HRP versus the wide applicability of hematin to different kind of substrates such as Alizarin and ARS. Hematin has demonstrated to be a very powerful oxidation catalyst for Alizarin in a previous work of our group, and also in this work for ARS.

This is one of the few comparative studies in which an enzyme (HRP) and its biomimetic (in this case hematin) are studied in comparative ways, using tools such as a very efficient experimental design (Doehlert) combined with a simple, but very useful, molecular modelling (MM2 + PM6). Hematin removes about 100% of ARS at 40 °C, pH 9.4, 1.1 mM of H_2O_2, and 4.4 mg hematin/l, whereas HRP only achieves 57% of ARS removal at 45 °C, pH 10.6, 3.2 mM of H_2O_2, and 2.5 mg HRP/l.

Regarding hydrogen peroxide effect an overall negative effect is observed on performances with both catalysts whereas inactivation mechanisms may be different. As evidenced by UV/vis spectra, structure modifications of hematin occur, either by formation of an inactive intermediate of hematin or by dimer formation. In case of HRP the appearance of inactive P670 species with high [H_2O_2] is clear. Hematin catalatic-like activity may account for oxygen evolution observed during reaction, thus being involved in the apparent yield recuperation with increasing H_2O_2 concentration. This observation cannot be applied to HRP since no oxygen evolution was observed during reaction.

Conformers resulting of the interaction of H_2O_2 and ARS with hematin and HRP Cpd-I were modelled and some substrate orientations were addressed as the most energetically favoured. Production of an active complex ARS-hematin Cpd-I may be straightforward with hematin. The lower ARS conversions observed with HRP compared to hematin are assigned, at least partially, to HRP inactivation. The inactivation reaction is supported by the theoretical calculations as related to the formation of bulky ARS dimers which inhibit the proper adsorption of substrate into the aromatic binding site in case of HRP Cpd-I. Moreover, the role of a coordinated water molecule in the neighbourhood of both catalytic structures was assigned as essential for catalytic activity, allowing reactivity of Cpd-I with bulky substrates in case of HRP.

Acknowledgments

Authors acknowledge the financial support of the National Council of Scientific and Technical Research (CONICET), the National Agency of Scientific and Technological Promotion (ANPCyT) and the National University of Córdoba (Argentina). We acknowledge the financial support granted through the PRH-03 and the PGI 24/Q022 SECyT-UNS (Bahía Blanca, Argentina). Furthermore, authors acknowledge the collaboration of the Chemical Industrial Department of the Faculty of Exact, Physical and Natural Sciences of the National University of Córdoba.

References

[1] J.A. Akkara, K.J. Senecal, D.L. Kaplan, J. Polym. Sci., Part A: Polym. Chem. 29 (1991) 1561–1574.
[2] A.M. Rao, V.T. John, R.D. Gonzalez, J.A. Akkara, D.L. Kaplan, Biotechnol. Bioeng. 41 (1993) 531–540.
[3] H. Puchtler, S.N. Meloan, M.S. Terry, J. Histochem. Cytochem. 17 (1969) 110–124.
[4] G. Liu, X. Li, J. Zhao, S. Horikoshi, H. Hidaka, J. Mol. Catal. A: Chem. 153 (2000) 221–229.
[5] J. Gao, J. Yu, Q. Lu, X. He, W. Yang, Y. Li, L. Pu, Z. Yang, Dyes Pigments 76 (2008) 47–52.
[6] D. Arrieta-Baez, R. Roman, R. Vazquez-Duhalt, M. Jiménez-Estrada, Phytochemistry 60 (2002) 567–572.
[7] S. Pirillo, F.S. García Einschlag, E.H. Rueda, M.L. Ferreira, Ind. Eng. Chem. Res. 49 (2010) 6745–6752.
[8] J. Karam, J.A. Nicell, J. Chem. Technol. Biotechnol. 69 (1997) 141–153.
[9] J.A. Nicell, J.K. Bewtra, K.E. Taylor, N. Biswas, C. St. Pierre, Water Sci. Technol. 25 (1992) 157–164.
[10] N. Vasileva, T. Godjevargova, D. Ivanova, K. Gabrovska, Int. J. Biol. Macromol. 44 (2009) 190–194.
[11] J. Cheng, S. Ming Yu, P. Zuo, Water Res. 40 (2006) 283–290.
[12] M. Shakeri, M. Shoda, J. Mol. Catal. B: Enzym. 54 (2008) 42–49.
[13] P. Peralta-Zamora, E. Esposito, R. Pelegrini, R. Groto, J. Reyes, N. Durán, Environ. Technol. 19 (1998) 55–63.
[14] H. Qayyum, H. Maroof, K. Yasha, Crit. Rev. Biotechnol. 29 (2009) 94–119.
[15] N. Durán, E. Esposito, Appl. Catal. B 28 (2000) 83–99.
[16] B. Meunier, Metalloporphyrin Catalyzed Oxidations, Kluwer Academic Publishers, Dordrecht, 1994.
[17] P. Zucca, F. Sollai, A. Garau, A. Rescigno, E. Sanjust, J. Mol. Catal. A: Chem. 306 (2009) 89–96.
[18] S. Nagarajan, R. Nagarajan, F. Bruno, L.A. Samuelson, J. Kumar, Green Chem. 11 (2009) 334–338.
[19] K. Ambrosio, E. Rueda, M.L. Ferreira, Biocatal. Biotransform. 22 (2004) 35–44.
[20] S. Saidman, E.H. Rueda, M.L. Ferreira, Biochem. Eng. J. 28 (2006) 177–186.
[21] J.C. Park, J.C. Joo, E.S. An, B.K. Song, Y.H. Kim, Y.J. Yoo, Bioresour. Technol. 102 (2011) 4901–4904.
[22] J.A. Shelnutt, J. Porphyr. Phthalocya. 4 (2000) 386–389.
[23] J.A. Shelnutt, in: K.M. Kadish, K.M. Smith, R. Guilard (Eds.), Porphyrin Handbook, Academic Press, 2000.
[24] C. Zazza, M. Aschi, A. Palma, Chem. Phys. Lett. 428 (2006) 152–156.
[25] G.H. Carlsson, P. Nicholls, D. Svistunenko, G.I. Berglund, J. Hajdu, Biochemistry 44 (2005) 635–642.
[26] J.N. Rodriguez-Lopez, M.A. Gilabert, J. Tudela, R.N.F. Thorneley, F. Garcia-Canovas, Biochemistry 39 (2000) 13201–13209.

[27] S. Tatoli, C. Zazza, N. Sanna, A. Palma, M. Aschi, Biophys. Chem. 141 (2009) 87–93.
[28] L.M. Colosi, Q. Huang, W.J. Weber Jr., J. Am. Chem. Soc. 128 (2006) 4041–4047.
[29] A. Henriksen, D.J. Schuller, K. Meno, K.G. Welinder, A.T. Smith, M. Gajhede, Biochemistry 37 (1998) 8054–8060.
[30] D.C. Montgomery, Design and Analysis of Experiments, 5th ed., John Wiley and Sons, New York, 2001.
[31] H. Gutierrez Pulido, R. De la Vara Salazar, in: D.F., Mexico, 2008.
[32] D. Doehlert, Appl. Stat. 19 (1970) 231–239.
[33] F. Benoit-Marquié, E. Puech-Costes, A.M. Braun, E. Oliveros, M.T. Maurette, J. Photochem. Photobiol. A: Chem. 108 (1997) 65–71.
[34] I. Magario, A. Neumann, E. Oliveros, C. Syldatk, Appl. Biochem. Biotechnol. 152 (2009) 29–41.
[35] M.M. Aslam, M.A. Baig, I. Hassan, I.A. Qazi, M.H. Saeed, Electron. J. Environ. Agric. Food Chem. (2004).
[36] M.I. Badawy, M.E.M. Ali, J. Hazard. Mater. 136 (2006) 961–966.
[37] European Commission, Integrated Pollution Prevention and Control (IPPC) Reference Document on Best Available Techniques for the Textiles Industry, European Commission, 2003.
[38] E.B.S.I.M. Kolthoff, E.J. Meehan, Stanley Bruckenstein, Análisis Químico Cuantitativo, 6° ed., Librería y Editorial Nigar S.R.L Buenos Aires, 1972.
[39] Berglund, G.H. Carlsson, A.T. Smith, H. Szoke, A. Henriksen, J. Hajdu, Nature (2002) 417–463, PDB ID:1H5A: G. I. http://www.rcsb.org/pdb/explore/explore.do?structureId=1h5a.
[40] G.I. Berglund, G.H. Carlsson, A.T. Smith, H. Szöke, A. Henriksen, J. Hajdu, Nature 417 (2002) 463–468.
[41] N.C. Veitch, Phytochemistry 65 (2004) 249–259.
[42] H.B. Dunford, Heme Peroxidases, John Wiley, VCH, USA, 1999.
[43] A.N.P. Hiner, E.L. Raven, R.N.F. Thorneley, F. Garcıía-Cánovas, J.N. Rodrıǐguez-López, J. Inorg. Biochem. 91 (2002) 27–34.
[44] J.J.K.T.L. Poulos, Biol. Chem. 255 (1980) 8199–8205.
[45] E. Derat, S. Cohen, S. Shaik, A. Altun, W. Thiel, J. Am. Chem. Soc. 127 (2005) 13611–13621.
[46] V. Schünemann, H. Winkler, Rep. Prog. Phys. 63 (2000) 263–353.
[47] E. Derat, S. Shaik, J. Phys. Chem. B 110 (2006) 10526–10533.
[48] P. Vidossich, G. Fiorin, M. Alfonso-Prieto, E. Derat, S. Shaik, C. Rovira, J. Phys. Chem. B 114 (2010) 5161–5169.
[49] J. Kulys, A. Ziemys, BMC Struct. Biol. 1 (2001) 3.
[50] S. Stewart, J.P. James, MOPAC Computational Chemistry, Colorado Springs, USA, 2009.
[51] J.J.P. Stewart, J. Mol. Mod. 13 (2007) 1173–1213.
[52] M.F. Nazar, A.M. Khan, S.S. Shah, J. Disper. Sci. Technol. 31 (2010) 596–605.
[53] A.T. Pilipenko, V.G. Safronova, V.V. Trachevsky, Ukr. Khim. Zh. 59 (1993) 399–404.
[54] B.B. Koleva, S. Stoyanov, T. Kolev, I. Petkov, M. Spiteller, Spectrochim. Acta, Part A 71 (2008) 847–853.
[55] G. Granados-Oliveros, F.M. Ortega, E. Páez-Mozo, C. Ferronato, J.M. Chovelon, Open Mater. Sci. J. 4 (2010) 15–22.
[56] G. Granados-Oliveros, E.A. Páez-Mozo, F. Martínez Ortega, M. Piccinato, F.N. Silva, C.L.B. Guedes, E. Di Mauro, M.F.D. Costa, A.T. Ota, J. Mol. Catal. A: Chem. 339 (2011) 79–85.
[57] G. Granados-Oliveros, E.A. Páez-Mozo, F.M. Ortega, C. Ferronato, J.M. Chovelon, Appl. Catal. B 89 (2009) 448–454.
[58] P. Zucca, C. Vinci, F. Sollai, A. Rescigno, E. Sanjust, J. Mol. Catal. A: Chem. 288 (2008) 97–102.
[59] J. Hernández-Ruiz, M.B. Arnao, A.N.P. Hiner, F. García-Cánovas, M. Acosta, Biochem. J. 354 (2001) 107–114.
[60] K.A. De Villiers, C.H. Kaschula, T.J. Egan, H.M. Marques, J. Biol. Inorg. Chem. 12 (2007) 101–117.
[61] M. Rafiquzzaman, K. Komagoe, K. Tamagake, Chem. Pharm. Bull. 43 (1995) 905–909.
[62] F.L. Emmert III, Thomas, J. Hon, B.A. Gengenbach, J. Inorg. Chim. Acta 361 (2008) 2243–2251.
[63] J. Ghasemi, S. Lotfi, M. Safaeian, A. Niazi, M.M. Ardakani, M. Noroozi, J. Chem. Eng. Data 51 (2006) 1530–1535.
[64] Y.L. Kapeluich, M.Y. Rubtsova, A.M. Egorov, Luminescence 12 (1997) 299–308.
[65] J.A. Nicell, K.W. Saadi, I.D. Buchanan, Bioresour. Technol. 54 (1995) 5–16.
[66] M. Wagner, J.A. Nicell, Water Res. 36 (2002) 4041–4052.
[67] T.E. Murphy, K.L. Tsui, J.K. Allen, Res. Eng. Des. 15 (2005) 201–215.
[68] M.A. Bezerra, R.E. Santelli, E.P. Oliveira, L.S. Villar, L.A. Escaleira, Talanta 76 (2008) 965–977.
[69] M.L. Foresti, M.L. Ferreira, Anal. Bioanal. Chem. 381 (2005) 1408–1425.
[70] A. Ziemys, J. Kulys, Int. J. Mol. Sci. 6 (2005) 245–256.
[71] L.G. Devi, K.E. Rajashekhar, K.S.A. Raju, S.G. Kumar, J. Mol. Catal. A: Chem. 314 (2009) 88–94.
[72] M. Panizza, M.A. Oturan, Electrochim. Acta 56 (2011) 7084–7087.
[73] H. Lachheb, E. Puzenat, A. Houas, M. Ksibi, E. Elaloui, C. Guillard, J.M. Herrmann, Appl. Catal. B 39 (2002) 75–90.
[74] A.M. Faouzi, B. Nasr, G. Abdellatif, Dyes Pigments 73 (2007) 86–89.
[75] J.A. Akkara, J. Wang, D.P. Yang, K.E. Gonsalves, Macromolecular 33 (2000) 2377–2382.
[76] N.A. Stephenson, A.T. Bell, Inorg. Chem. 46 (2007) 2278–2285.
[77] N.A. Stephenson, A.T. Bell, J. Am. Chem. Soc. 127 (2005) 8635–8643.
[78] S. Pirillo, F.S.G. Einschlag, M.L. Ferreira, E.H. Rueda, J. Mol. Catal. B: Enzym. 66 (2010) 63–71.
[79] M.L. Ferreira, Macromol. Biosci. 3 (2003) 179–188.
[80] P.R. Rich, M. Iwaki, Biochemistry (Moscow) 72 (2007) 1047–1055.
[81] G.H. Loew, D.L. Harris, M. Dupuis, J. Mol. Struct.: Theochem. 398–399 (1997) 497–505.
[82] N. Marom, A. Tkatchenko, S. Kapishnikov, L. Kronik, L. Leiserowitz, Cryst. Growth Des. 11 (2011) 3332–3341.
[83] F. Xu, D.E. Koch, C.K. In, R.P. Hunter, A. Bhandari, Water Res. 39 (2005) 2358–2368.
[84] S. Daré-Doyen, D. Doizi, P. Guilbaud, F. Djedaïni-Pilard, B. Perly, P. Millié, J. Phys. Chem. B 107 (2003) 13803–13812.